MODELLING OF A WAVE FLUME IN ANSYS FLUENT

by

Jianxin Liu
/R63D2Y/

Submitted to the
Department of Fluid Mechanics of the
Budapest University of Technology and Economics
in partial fulfillment of the requirements for the degree of
Master of Science in Mechanical Engineering Modelling

on the 11th of December, 2020

MSc Thesis

Final Project B /BMEGEÁTMWDB/

Supervisor:
Josh Davidson, PhD, research assistant

Department of Fluid Mechanics
Faculty of Mechanical Engineering
Budapest University of Technology and Economics

DECLARATION

Full Name (as in ID):	Liu Jianxin
Neptun Code:	R63D2Y
University:	Budapest University of Technology and Economics
Faculty:	Faculty of Mechanical Engineering
Department:	Department of Fluid Mechanics
Major/Minor:	MSc in Mechanical Engineering Modelling Fluid Mechanics major / Solid Mechanics minor
	Thesis Title: Modelling of a Wave Flume in ANSYS Fluent
Academic year of submission:	2020 / 2021 - I.

I, the undersigned, hereby declare that the Thesis submitted for assessment and defence, exclusively contains the results of my own work assisted by my supervisor. Further to it, it is also stated that all other results taken from the technical literature or other sources are clearly identified and referred to according to copyright (footnotes/references are chapter and verse, and placed appropriately). I accept that the scientific results presented in my Thesis can be utilised by the Department of the supervisor for further research or teaching purposes.

Budapest, on the 17th of December, 2020

_____

(Signature)

FOR YOUR INFORMATION

The submitted Thesis in written and in electronic format can be found in the Library of the Department of Fluid Mechanics at the Budapest University of Technology and Economics. Address: H-1111 Budapest, Bertalan L. 4-6. “Ae” building of the BME

ACKNOWLEDGEMENT

“It’s simple: overspecialize, and you breed
in weakness. It’s slow death.”
—Ghost in the shell (1995)

I would like to thank my supervisor Josh Davidson for his patient guidance and support in the creation of this thesis. I would like also to thank my supervisor for his help with any questions I had during the creation of this thesis.

Furthermore I would like to thank my family and friends for their faith in my ability to deliver this thesis.

ABSTRACT

This thesis will involve development of a Numerical Wave Tank (NWT) using ANSYS Fluent. The NWT has already been under development using the Open-Source CFD software OpenFOAM, for the purpose of testing and optimising marine renewable energy devices, such as wave energy converters. This thesis have analysed experimental data of regular and focused wave kinematics from a test campaign conducted in July 2018 in the COAST laboratory in Plymouth University, UK, Then establish a two-dimensional numerical wave tank according to the entity of the wave flume in the experiment, and realize the verification of the NWT experiment results by comparing the numerical result with the experimental data.
In the experiment, the resistance wave probe was used to measure the free surface elevation and the particle image velocimetry (PIV) to measure the particle velocity. The first set of simulation is performed on regular waves, and it is expected that the simulation settings will be verified by comparing the results with the expected Stokes theory. And also made a verification of wave maker. It is found that NWT can produce the desired wave shape very well by using dynamic grid technology to simulate the motion of the wave maker.
The second set of simulation was performed on focused waves. Compared the free surface elevations at different locations between the numerical results and experimental data. It can be found that the numerical results don't have a good agreement with the experimental data along the wave tank to reproduce the process of the wave focusing. Because there is a large error between the amplitude of the free surface elevation of numerical wave tank and experimental results. So the NWT was not able to accurately reproduce the focused waves tested experimentally in the wave flume.

KIVONAT (ABSTRACT IN HUNGARIAN)

Ez a tézis egy numerikus hullámtartály (NWT) fejlesztését foglalja magában az ANSYS Fluent alkalmazásával. Az NWT már fejlesztés alatt állt az OpenFOAM nyílt forráskódú CFD szoftverrel, a tengeri megújuló energiát használó eszközök, például hullámenergia-átalakítók tesztelésére és optimalizálására. Ez a tézis elemezte a 2018 júliusában a COAST laboratóriumában, az Egyesült Királyságban található Plymouth University-ben végrehajtott tesztkampány szabályos és fókuszált hullámkinematikájának kísérleti adatait, majd létrehozott egy kétdimenziós numerikus hullámtartályt a kísérletben szereplő hullámáram entitásának megfelelően. , és valósítsa meg az NWT kísérleti eredmények ellenőrzését a numerikus eredmény és a kísérleti adatok összehasonlításával.
A kísérlet során az ellenálláshullám-szondát használtuk a szabad felület magasságának mérésére, és a részecskekép-sebességmérést (PIV) a részecskék

sebességének mérésére. Az első szimulációs készletet szabályos hullámokon hajtják végre, és várhatóan a szimulációs beállításokat az eredmények és a várható Stokes-elmélet összehasonlításával fogják ellenőrizni. És ellenőrizte a hullámkészítőt is. Megállapítást nyert, hogy az NWT nagyon jól képes előállítani a kívánt hullámformát azáltal, hogy dinamikus rács technológiával szimulálja a hullámkészítő mozgását.
A szimuláció második sorozatát fókuszált hullámokon hajtották végre. Összehasonlítva a szabad hely magasságát a különböző helyeken a numerikus eredmények és a kísérleti adatok között. Megállapítható, hogy a numerikus eredmények nem egyeznek jól a hullámtartály menti kísérleti adatokkal a hullám fókuszálásának folyamatának reprodukálásához. Mivel nagy hiba van a numerikus hullámtartály szabad felületi magasságának amplitúdója és a kísérleti eredmények között. Tehát az NWT nem tudta pontosan reprodukálni a kísérletileg tesztelt fókuszált hullámokat a hullámárban.

NOMENCLATURE

- t , time (s)
- ρ , density ($\mathrm{kg}.m^{-3}$)
- v , velocity vector ($m.s^{-1}$)
- T, τ , viscous stress tensor ($N.m^{-2}$)
- μ , dynamic viscosity ($Pa.s$)
- μ_t , turbulent viscosity ($Pa.s$)
- V , volume (m^3)
- k , turbulent kinetic energy ($m.s^{-2}$)
- ε , turbulent dissipation ($m^2 \cdot s^{-2}$)
- ω , specific turbulent dissipation (s^{-1})
- p , pressure (Pa)
- f ,wave frequency (Hz)
- f_b , peak frequency (Hz)
- u , horizontal component of velocity vector ($m^{-1}.s^{-1}$)
- v , vertical component of velocity vector ($m^{-1}.s^{-1}$)
- g , gravitation acceleration ($m.s^{-2}$)
- k , wave number (m^{-1})
- α , volume fraction (-)
- η , free surface elevation (m)
- L ,wavelength(m)
- A , wave amplitude (m)
- d ,water depth (m)
- T , wave period (s)

Acronyms

ADV	Acoustic Doppler Velocimetry
CFD	Computational Fluid Dynamics
CNWT	CFD-based Numerical Wave Tank
LDV	Laser Doppler Velocimetry
NWT	Numerical Wave Tank
PIV	Particle Image Velocimetry
PM	Pierson-Moskowitz
WEC	Wave Energy Converter
WP	Wave probe
FFT	Fast Fourier Transform
WSI	wave solid interaction
FDM	finite difference method
BEM	Boundary Element Method
FVM	Finite Volume Method

CONTENTS

1 Introduction

There are two forms of energy resource consumption on earth. The first one are non-renewable energy sources with significant consumption of coal, crude oil and natural gas. With the exploration and utilization of new energy in many countries in recent years, especially in the so-called renewable sources, so the other one are renewable sources such as wind, solar and hydro-power that is represented in a finding shown on Fig.1. With the limited supply of non-renewable sources of energy, we have to not only just maintain, but also research and develop other ways of renewable energy production for the future generation.

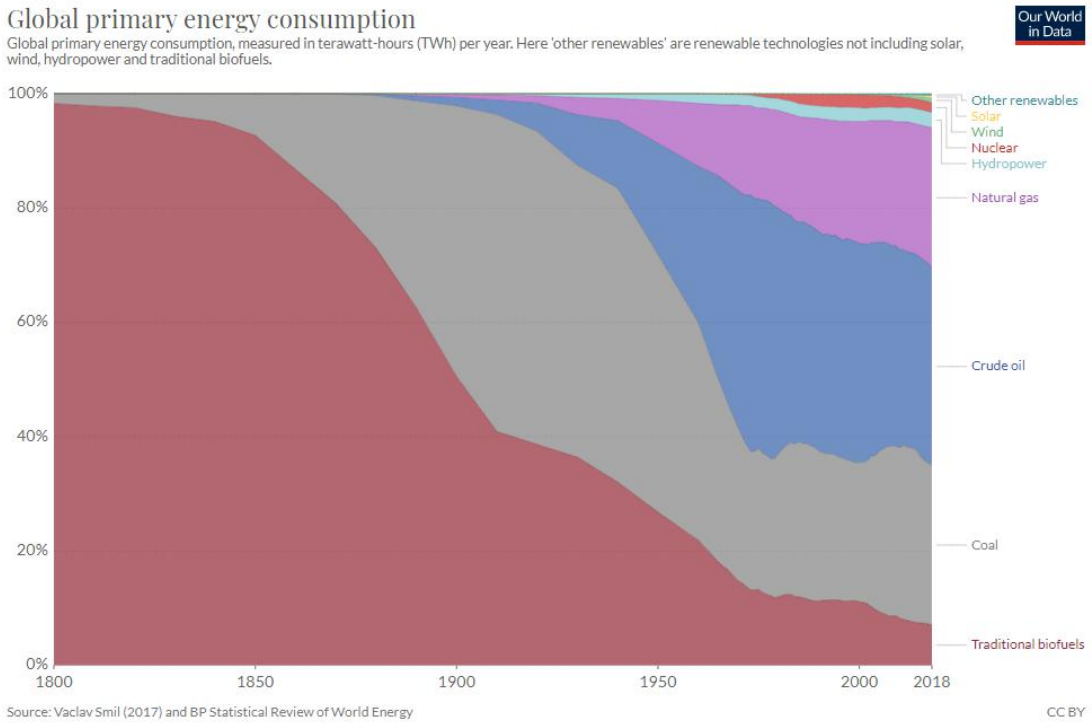

Fig. 1: World wide energy consumption [1]

Compared to other renewable energy, within the ways of other renewable energy sources, one of those that has been highlighted is Marine Energy. It also known as Marine Renewable Energy (MRE)As we know, seventy percent of the Earth's surface is covered by the oceans, which contain vast amount of energy in various forms. The oceans contain the biggest of natural resources and have a huge energy potential can contribute to the growing energy needs in the earth. We already employ various methods to harness the energy of our oceans and seas to get different energy , including tidal stream, offshore wind, ocean thermal and current energy.

By using devices to converting the energy of sea waves into other energy resources, it is important for us. Wave Energy Converters (WEC) is a device of MRE to capture the mechanical motion of the sea waves and convert it to other form of power such as electricity. Although we can choose a variety of electrical energy for WEC to generate,

WEC is designed to generate electricity is a normal form, because it is being recognized as the easiest form of energy to exploited for the sustainable generation of electrical power.

1.1 Wave Energy Converters (WEC)

WECs have been developed to extract energy from shoreline out to the deeper waters offshore. These devices are generally categorized by the installation location and the Power Take-Off (PTO) system. Locations are shoreline, near shore and offshore (Fig. 2). [2]

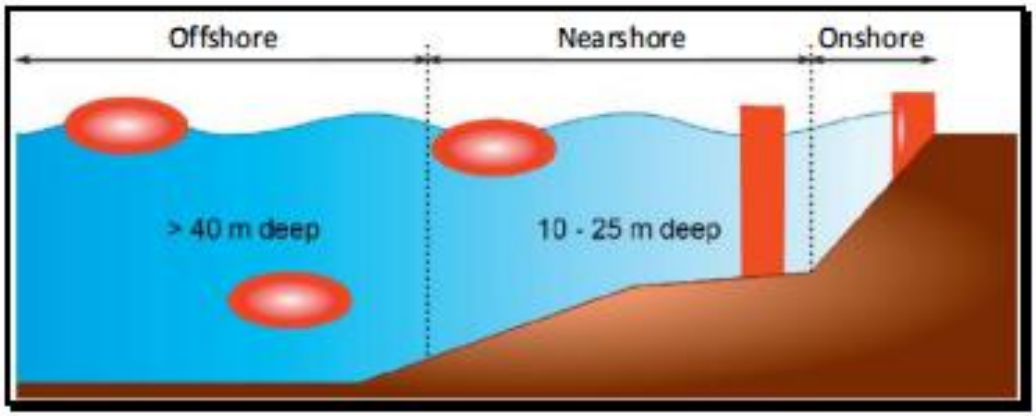

Fig. 2: WECs location [2]

In this context, most devices can be characterized as belonging to six types: Attenuator; Point absorber; Oscillating wave surge converter; Oscillating water column; Overtopping device; Submerged pressure differential. Fig.3 summarizes the main WEC projects in terms of concepts and locations [2].

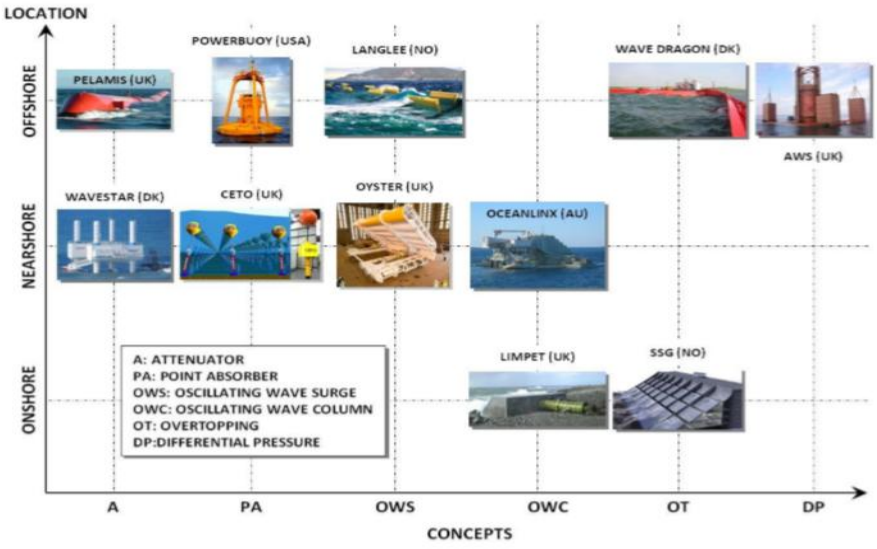

Fig. 3: WEC main projects [2]

The following introduction of some converters from a review of wave energy converter technology [3].

1.1.1 Attenuator

Attenuator lie parallel to the predominant wave direction. It is a snake-like appearance, each section is connected by a joint that allows the attenuator to undulate along each wave, the movement of the wave pushes and pulls hydraulic cylinders causing fluids to compress into the high pressure accumulators creating an electrical current. As shown in Fig.4a.

1.1.2 Point absorber

A point absorber is a device that possesses small dimensions relative to the incident wavelength. They can be floating structure that heave up and down on the surface of the water or submerged below the surface relying on pressure differential. Because of their small size, wave direction is not important for these devices [2]. Fig.4b shown how it works in the surface of sea.
It works using a buoy that floats above the water to generate power. A giant shaft is anchored to the sea floor with the buoys secured on top as the buoy moves up and down with the waves the pumping action is converted into electricity.

1.1.3 Submerged pressure differential

The submerged pressure differential device is a submerged point absorber that uses the pressure difference above the device between wave crests and troughs. It comprises two main parts: a sea bed fixed air-filled cylindrical chamber with a moveable upper cylinder. As a crest passes over the device, the water pressure above the device compresses the air within the cylinder, moving the upper cylinder down. As a trough passes over, the water pressure on the device reduces and the upper cylinder rises.As shown in Fig.4c.

1.1.4 Overtopping

An overtopping device captures sea water of incident waves in a reservoir above the sea level, then releases the water back to sea through turbines. Overtopping works like this, when a wave approaches the rig to wave reflectors ,guide the water to the center and up a curved ramp into the reservoir where the water is stored. There are several hydro turbines , the water pressure spins the turbines and the energy is converted into electricity with a magnetic generator.
An example of such a device is the Wave Dragon, which is shown in Fig.4d. This device uses a pair of large curved reflectors to gather waves into the central receiving part, where they flow up a ramp and over the top into a raised reservoir, from which the water is allowed to return to the sea via a number of low-head turbines.

1.1.5 Oscillating wave surge converter

An oscillating wave surge converter is generally comprised of a hinged deflector, positioned perpendicular to the wave direction (a terminator), that moves back and forth exploiting the horizontal particle velocity of the wave. An example is the Aquamarine Power Oyster a nearshore device, where the top of the deflector is above the water surface and is hinged from the sea bed. A prototype of this device has been constructed. Fig. 4e illustrates the device.

1.1.6 Oscillating water column

An closed chamber has an opening beneath sea level which allows water to flow from the sea to the chamber and back. The water level in the chamber rises and falls with the rhythm of the waves and air is forced forwards and backwards through the turbine connected to an upper opening in the chamber. As it is compressed and decompressed the airflow has sufficient power to drive the Wells turbine. It is driven in the same direction by both forward and reverse air flow through the turbine. It is shown in Fig. 4f.

a) Attenuator

b) Point absorber

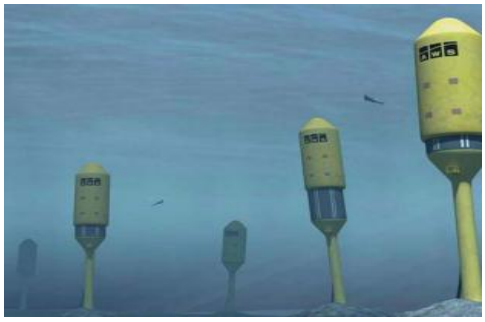

c) Submerged pressure differential

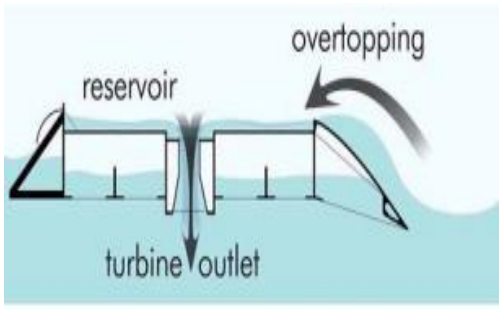

d) Overtopping

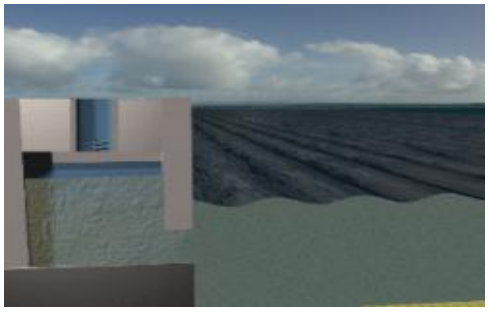

e) Oscillating wave surge f) Oscillating water column

Fig.4: Types of Marine Energy Converters [3]

The development of WECs encapsulates major part of fluid dynamics and with complex consideration of many aspects of computational fluid dynamics (CFD) is employed. Numerical Wave Tanks (NWT) are set up to simulate the fluid-solid interaction between WECs and ocean wave motion, in many cases the interaction is abbreviated as wave solid interaction (WSI) for wave-solid interaction to differentiate the topic from the general definition. Testing and optimizing NWTs has been under development for years and many commercial toolbox is available to perform the required simulations.

However the implementation of WECs in NWTs with computational solvers new challenges surface with accuracy of the simulation, computational cost, hardware cost and last but least the licensing cost of the chosen software.

1.2 Wave Theories

There are many types and shapes of waves on the earth. But this thesis mainly studies ocean waves. Ocean waves are mainly generated by the action of wind on water. The waves are formed initially by a complex process of resonance and shearing action, in which waves of differing wave height, length, period are produced and travel in various directions. Water waves can be described in Fig.5 using the main characteristics of waves [4].

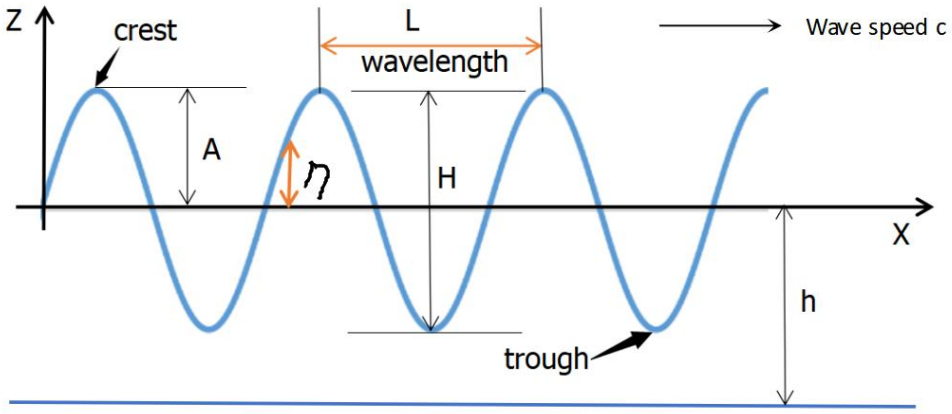

Fig.5: Characteristics of waves

L [m] is the wavelength (distance between successive crests), T [s] is the wave period (time interval between successive crests passing a particular point), A [m] is the wave amplitude, which is vertical distance between the still water level and a crest or a trough, but we have to note that the crest amplitude and the trough amplitude are different for non-linear wave, η [m] is called the free surface elevation (distance between the still water level and the wave surface), H [m] is the wave height that can be described the vertical distance between crest and trough, h[m] is the depth (distance from the seabed to the mean sea level), f [Hz] is the wave frequency, which is explained as corresponds to the number of repeating patterns in one second. W is the inverse of the wave period, Some commonly used calculation formulas for waves be calculated by the following equation:

- Angular frequency ω [rad.s^{-1}], $\omega = 2T\pi$.
- Wave number k [mm1]: $k = 2\lambda\pi$
- Phase velocity (wave speed, wave celerity) c [m.ss1]: propagation velocity of the wave form $c = \lambda/T$.
- Wavelength L [m]: $L = \frac{gT^2}{2\pi}\tanh\left[\frac{2\pi h}{L}\right]$

where g is the acceleration due to gravity,T [s] is the wave period.

1.3 Outline of the thesis

This project will involve development of a Numerical Wave Tank (NWT) using ANSYS. The numerical wave tank (NWT) has already been under development using the Open-Source CFD software OpenFOAM, for the purpose of testing and optimising marine renewable energy devices, such as wave energy converters. A NWT is required in the CFD simulation of an OWC device.Wave probes are a very common device used to measure the height of a surface in the experiment, but wave gauges can be implemented to measure the wave height in the simulation of wave tank.

This final thesis aims to accomplish a comparison between experimental data and numerical results that from an NWT in the commercial CFD software Ansys Fluent. At the beginning of the research, an introduction of wave application and the characteristics of waves in Chapter 1. Then in Chapter 2 the concept of physical wave tank and numerical wave tank (NWT) are given, especially numerical wave tank is detailed. After that, the section is a case study, including the setup of experiment, measuring equipment were used in the experiment, and an detailed introduction of regular wave and focused wave In Chapter 3.

The core part of this thesis is the ANSYS NWT in Chapter 4, firstly, proper NWT geometry was defined, which is appropriate for the wave tank of simulation from the case study, then The detailed process of the entire simulation will be fully introduced, such as the geometry, the wave parameters and the generation of the waves and the applied turbulence models and simulation settings are presented. And a short literature review was carried out, where the applied turbulence models of this field.

Furthermore, the method of simulation: Volume of Fluid model (VOF), which is a surface-capturing method for multiphase flows, and the wave makers also was studied. Chapter 5 contain the regular waves and the focused wave results of the simulation respectively. The conclusions are summarized in Chapter 6. At the end of the thesis, the summery is presented.

2 Wave tank

The first part of this section summarizes the concept of the physical wave tank, which is used in the experimental study. Secondly, the concept of numerical wave tank is detailed in the second part of this section. Thirdly, summarizes the required technical background on numerical wave tank.

2.1 Physical wave tank

The physical wave tank is usually a laboratory setup for observing the behavior of surface waves. A typical wave tank is a box filled with liquid (usually water) with an open space at the top of the tank. At one end of the tank, a wave maker will be used to generates waves; the other end usually has a wave-absorbing device to absorb waves. The wave basin is a three-dimensional model commonly used for testing ships, offshore structures and ports (and their breakwaters). It is a wave tank with comparable width and length.A physical wave tank picture is shown in Fig.5.[5]
A wave flume (or wave channel) is a special sort of wave tank: the width of the flume is much less than its length. The generated waves are two-dimensional in a vertical plane, which means that the orbital flow velocity component in the direction perpendicular to the flume side wall is much smaller than the other two components of the three-dimensional velocity vector. So wave flumes may be used to study the effects of water waves on coastal structures, offshore structures, sediment transport and other transport phenomena. Waves are usually generated by mechanical wave generators. Modern wave generators are computer-controlled. In addition to periodic waves, they can also generate random waves, solitary waves, wave groups and even tsunami-like waves. The wave maker is located at one end of the wave trough, and the other end is the structure or absorber under test (beach or special wave absorbing structure).[5]

Fig.5: Physical wave tank[5]

2.2 Numerical wave tank

With the development of computer technology，the application of the numerical wave tank (NWT) which can partly substitute physical model test to investigate wave body problem has become more and more important. The emergence of CFD software FLUENT based on Navier-Stokes equations makes the realization of numerical wave tank possible.

Numerical Wave Tank (NWT) is a general term for numerical simulators that can simulate nonlinear free surface waves, hydrodynamics and floating body motion. In general, the computational fluid dynamics (CFD) method can solve the non-simplified Navier-Stokes equations in the case of considering the fluid viscosity, so it is most important that the NWT provide results with an appropriate degree of accuracy to ensure that results from subsequent modelling are not distorted or diminished. However, the computational burden related to the CFD algorithm is heavy. Fortunately, after continuous improvement, CFD is now effectively embedded in the field of marine engineering. [6]

2.2.1 Numerical wave flume simulation method

Because numerical wave tank is very important to wave research and scientific development, the commonly used calculation methods, such as finite difference method, finite element method, boundary element method, finite volume method, etc., have been used in the simulation of wave numerical flume.

2.2.1.1 FDM

The earliest numerical method in history is the finite difference method (FDM), which is the most classic and can directly deal with unsteady Navier-Stokes equation (NS equation) is solved, but FDM must have many assumptions to realize numerical simulation. Moreover, FDM must divide the grid points very densely, and the number of grid points may increase by a power number. This places extremely high requirements on the computing and storage capabilities of the computer, which greatly consumes computer memory, and it is difficult for FDM to simulate moving boundaries. And irregular borders. The finite element method (FEM) can make up for the weakness of FDM. FEM can freely divide the density of grid points, and it can also solve the problem of moving boundaries. It divides the calculation area into a series of unit bodies, each unit body takes several nodes, and the equations are discretized by integrating the governing equations at the nodes. Some results have been obtained by using finite element method to simulate wave numerical flume. Through the study of second-order Stokes waves, the rationality of the wave numerical flume was clarified. FEM can solve the calculation of irregular areas, its adaptability is better, but the calculation. The workload is still very large, so the boundary element method is not the finite element method used in the study of wave numerical flume calculation.

2.2.1.2 BEM

The Boundary Element Method (BEM) transforms the basic solution of the differential equation into an integral equation at the boundary, and then solves the integral equation to obtain the solution of the differential equation. BEM has far more advantages than FEM. The boundary element method satisfies the Laplace equation in a closed area. The existence of the basic solution of the Green function means that the value at any point in the area can be obtained from the value at the boundary. The solution of the boundary element method only needs to discretize the boundary of the wave flume, and then the solution in the entire flow field area can be obtained. This is an important advantage of BEM, which is the "dimension reduction advantage", which greatly simplifies the calculation steps. Obviously, the boundary element method can be applied to the boundary of any shape. In addition to the advantage of dimensionality reduction, it also has high accuracy. However, the boundary element method also has shortcomings. The most important thing is that its application range is based on the existence of the basic solution of the corresponding differential operator. It is difficult to apply to non-uniform media, so its application range is relatively limited. Moreover, the coefficient matrix of algebraic equations usually established by it is an asymmetric full matrix, which limits the speed and scale of problem solving. For nonlinear problems, if the in-domain integral term in the equation will partially offset the advantages of the boundary element method.

2.2.1.3 FVM

Finite Volume Method (FVM) is a new research Navier-Stokes. The numerical calculation method of Stokes equation is currently widely used in problems such as flow, heat transfer, and radiation.It divides the computational domain into a series of control bodies. The characteristics of each control body are represented by a node at the centroid. A discrete control equation is established by establishing a flux conservation equation at the node of the control body. Because the discrete form obtained by FVM has the characteristics of conservation, the physical meaning of its discrete coefficients is also clearer. With the rapid development of computer technology, a variety of software has emerged, in the calculation software based on the finite volume method. Among the many softwares of computational fluid dynamics, FLUENT is currently the most widely used. It is based on a completely unstructured grid and uses a finite volume method software that implements a gradient algorithm on the nodes and elements of the grid. FLUENT software uses a variety of grids, such as discontinuous grids, dynamic grids, sliding grids and hybrid grids, etc. At the same time, the grid has many advantages such as white adaptability.

2.2.2 CNWT

CFD is a computer-based mathematical modeling tool that combines basic fluid flow equations Navier-Stokes equations and other related equation solutions. The Navier-Stokes equation expresses the law of conservation of mass, momentum and energy in differential form. Then these integral forms of partial differential equations

are approximated to finite volume expressions, and then converted into algebraic equations for numerical calculation. In the specified domain. The FLUENT software used in this study uses the finite volume method to solve the Navier-Stokes equations and has multiple functions applicable to the current problem of multiphase flow. These functions include the ability to implement the VOF method to track the air-water interface in the domain. This is not only an important means of describing the interface, but also essential for the correct modeling of the hydraulic-pneumatic interaction in the OWC chamber.

In CFD's NWT (CNWT), the Navier-Stokes equation is restored by using time steps and grids to discrete time and space domains, respectively. CNWT have a number of features when it is applied in the field of marine engineering. A review of all the characteristics of CNTW is summarized by Windt et al. [7]. CNWT has three main characteristics: wave generation and wave absorption methods and fluid-structure coupling. Generally, in a 2D simulation, a wave is generated at one end of the tank, and wave absorption is generated at the other end to avoid accidental reflection of the wave from the wall. In only numerical wave simulation for wave motion analysis, since the focus of wave kinematics is that no objects are added to the domain, only wave generation and wave absorption are required. The location of the simulation area is far enough away from the wave generator to ensure that the waves are fully expanded and all vanishing waves disappear. Nowadays, it is still a challenge to generate the correct wave in the simulation area with minimum reflectivity.

There are many methods for generating and absorbing waves, which are reviewed and discussed in [8]. Wave maker methods can be divided into two different categories: some wave makers replicate the behavior of experimental wave makers, such as pistons or paddles. The second category allows the generation of higher-order waves and avoids the inherent errors of the experimental equipment, such as evanescent waves, imperfect wave absorption, and necessary control of the wave generator. In the experiment, the Impulse Source Wave Maker (ISWM) was implemented. In the simulation, wave making is achieved by dynamic grid method. Details are given in Section 4.4. Wave absorbtion can also be achieved by different means. The ISWM is associated with numerical beaches which ensure wave absorption to any desired reflection coefficient in the experiment, but it have to at great computational cost. So in this thesis, only the generation of waves is simulated, but the absorption of waves is not realized.

NWT is just a basic building block to which various functions that need to be considered (for example, OWC) can be added. But in this thesis, nothing is added. Using CFD to analyze any fluid flow is an iterative process, including three basic steps: First of all, numerical field settings(Including geometry generation, meshing, turbulence model selection); secondly, modeling and calculation(simulation setting and calculation type selection); finally, results evaluation (For example, comparison of simulation results and experimental data of wave height and speed).

2.3 VOF method

The numerical model used is based on the volume of fluid (VOF) method, which allows the calculation of the wave box by observing the interaction between water and air. The VOF method can simultaneously track the volume of the two fluids in the entire volume by converting the motion equation Fractions are used to model two immiscible fluids. In each control volume, the sum of the volume fractions of all phases is single. Each stage shares a breakdown of all variables and attributes, and represents the minimum volume, as long as the volume fraction of each stage is known locally. Therefore, in order to determine the value of the volume fraction, the variables and characteristics in a given volume represent one of the phases or the complement of the phases.

The Volume of Fluid method (VOF) is a surface capture method that can describe and store information about the volume fraction of liquid in a cell with only one storage word. Therefore, the VOF method requires the same storage requirements as other dependent variables. By implementing the VOF method into our numerical model, the discrete governing equation contains an additional scalar field f to describe the volume fraction of fluid in the cell. When the cell is filled with field-related fluid, the value of f is equal to 1, and when the cell does not contain any fluid, the value of f is equal to zero. In addition, when the cell is only partially filled with the fluid, the value of f can be between zero and one. Therefore, the free surface of the fluid related to the field can be located.

In the case of NWT, the interaction of water and air, multiphase flow involves two or more fluid phases. During the simulation, it is also important to track the position of the interface between the two fluids. The flow field in the liquid phase is usually calculated by appropriately considering the kinematics and dynamic boundary conditions at the interface. To deal with this type of interaction, one accepted method is the volume of fluid (VOF) method. The VOF model depicting free surface interface shown in figure 6.[9]

In the VOF model, the calculation of a single fluid whose density and viscosity are averaged according to the volume fraction of each phase:

$$\rho = \alpha_l \rho_l + (1 - \alpha_l)\rho_g$$

$$\mu = \alpha_l \mu_l + (1 - \alpha_l)\mu_g$$

where α_l is a volume fraction of liquid, α_g volume fraction of gas and ρ_l and ρ_g are densities of liquid and gas respectively. Velocity also determined on weighted-average method as:

$$v = \frac{\alpha_l \rho_l v_l + \alpha_g \rho_g v_g}{\rho}$$

Since the VOF model is usually used for separate streams, each stage in each domain can be processed accurately. Flow and fluid properties are applied only at the interface. In order to maintain a clear interface, the interface will be refactored after each time

step. The position of the interface is obtained from the volume fraction equation of stage k:

$$\frac{\partial \alpha_k}{\partial t} + \nabla \cdot (\alpha_k v) = 0$$

$$\sum_{k=1}^{n} \alpha_k = 1$$

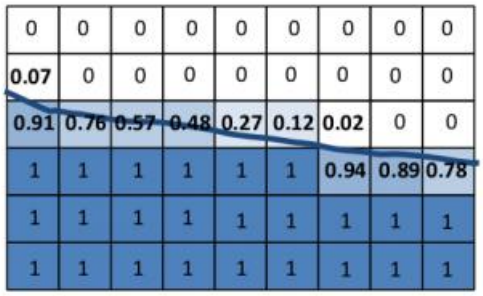

Fig.6: VOF model depicting free surface interface [10]

3 Case study

3.1 Experiments

The experiment was carried out in a 35m long, 0.6m wide and 0.7m deep sedimentation tank in the COAST laboratory of the University of Plymouth, UK. A schematic diagram of the experimental setup is given in Figure 7. The wave tank is equipped with Edinburgh-designed wave-making machine paddles. At the end of the wave trough, an absorbent beach was installed. Eight wave probes (labeled WP in Fig.7) are installed in the tank. The photo in Fig.8 shows a regular wave propagating along the tank. You can see the ADV probe in the lower left corner, the PIV camera in the lower right corner, and some wave probes in the middle of the picture. The wave probe 3 is located in the center of the PIV query window (green color code in Fig.7). Wave probes 4–8 are installed to allow the analysis of wave reflection.[6]

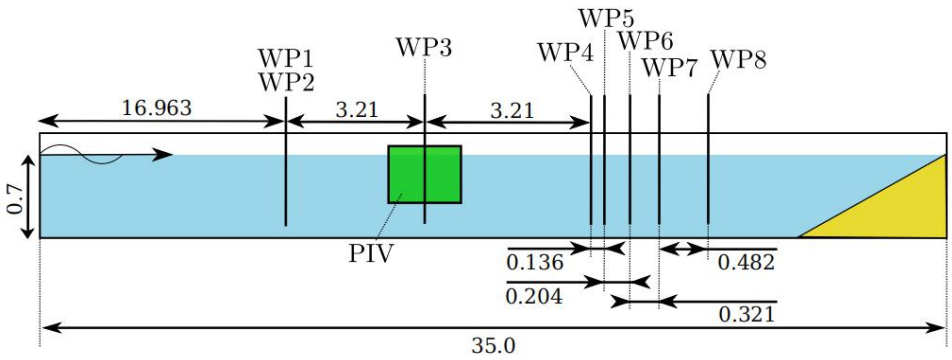

Fig.7: Wave tank schematic [6]

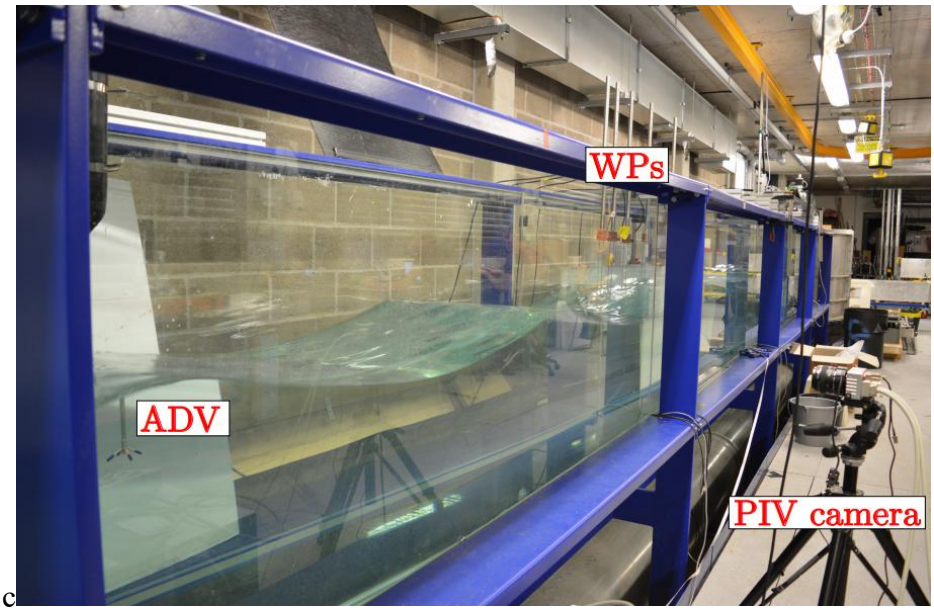

Fig.8: Photograph of the flume [6]

3.2 Measuring equipment

3.2.1 Resistive wave probes

The wave probe is a very common device used to measure the height of a surface. In the experiment of this research, eight resistance wave probes (WP) were used to track the free surface. These probes are made of two parallel vertical wires and are immersed in water. The conductivity between two wires is related to the depth of immersion, and the resistance between the wires is proportional to the depth of immersion, so the height of the free surface at a certain position of the water tank can be measured. Wave probe 1 and 2 closest to the wave maker blades are at the same horizontal distance from the wave maker, and the exact position should be 16.96m. The wave detector 1 is located on the center line of the wave trough, and the wave detector 2 moves to the rear wall. The other wave probes 3-8 are all aligned with the center line of the direction of wave propagation and maintain the same horizontal line as the wave detector 1. Install wave probes 4-8 to determine the reflection coefficient in the direction of wave propagation. For better visibility, the distances between wave detectors 1-8 are listed in Table1.The photo in Fig.9 showing the high-speed camera for the PIV measurements and the wave probes.[6]

Table 1: Distances between wave probes 1–8

Distances between wave probes 1–8 [m]						
Movingwall-WP1	WPs1,2-3	WPs3-4	WPs4-5	WPs5-6	WPs6-7	WPs7-8
16.963	3.21	3.21	0.136	0.204	0.321	0.482

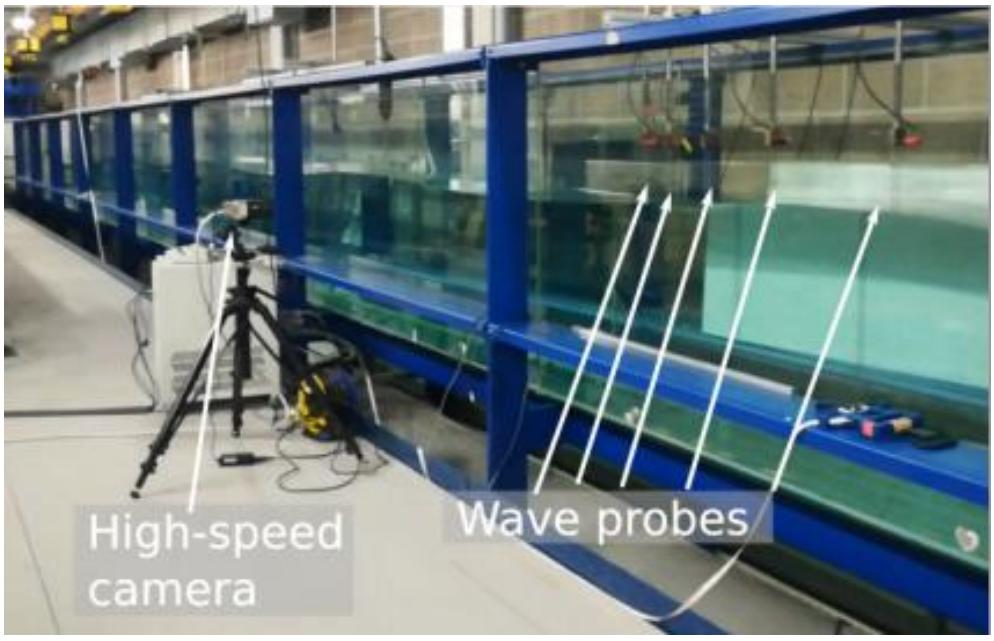

Fig.9: Photograph of wave probes [6]

3.2.2. Particle image velocimetry (PIV)

Particle Image Velocimetry (PIV) is an optical method often used for flow visualization for education and research. It is used to obtain instantaneous velocity measurements and related properties in the fluid. Since PIV allows velocity measurement in the form of points, lines or fields, so the particle image velocimetry (PIV) method is widely used to measure the wave kinematics on the vertical surface of the experimental wave box. And this method also becomes a powerful tool for validating CFD simulations in many researches.[6]

The principle of detailed PIV will not be introduced here. Just a brief introduction about it : PIV allows the use of continuous image pairs of small tracers suspended in water to measure the instantaneous horizontal and vertical velocities in the water flow. It's means that 2D visualization is allowed. Of course, it also can be in 3D. The high-speed camera is used for capture images of the illuminated flow in this study. A thin laser beam illuminates the flow on a certain area to ensure a good display of the tracer.

It is worth noting that when setting up PIV measurement, first of all, the same particles should appear in a pair of images. However, because the flow is moving forward, the interrogation window must be moved or distorted to follow the particle pile. Secondly, background noise will change the result, so it must be styled before performing cross-correlation, Finally, particles cannot travel with perfect 2D motion, so they can move out of the interrogation window. The main features of a general PIV experimental setup are presented in Fig.10.[6]

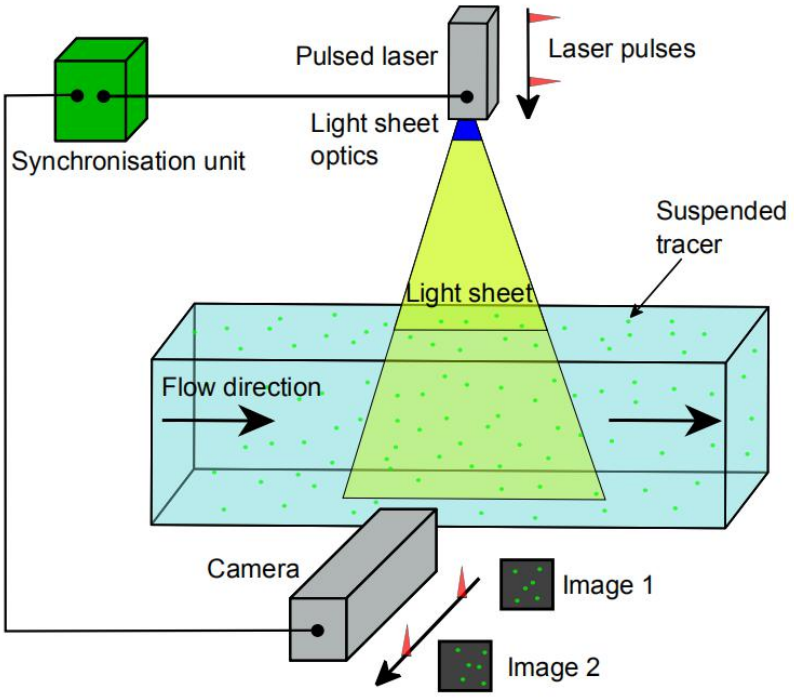

Fig.10: Key elements of a PIV system [6]

3.2.3 Velocity point measurements

Acoustic Doppler Velocimetry (ADV) is used to record single point instantaneous velocity components at relatively high frequencies. The measurement is performed by the particle velocity in the remote sampling volume measured based on the Doppler shift effect. This equipment has been used in the experimental work. The ADV probe used in this study is the Nortek Vectrino device.To give a brief introduction to the working principle of the device, in this particular device the transmitter generates a sound wave pulse, which is reflected on the scattering material in the dating water. Water does not reflect sound waves, so suspended particles that move with the water flow are needed. Frequency change between waves. This change in frequency is related to the speed of the particles.[6]

3.3 Regular wave

Regular waves are called gravity waves (also called surface waves). Gravity waves are understood as clear regular waves of behavior, according to their constant characteristics in each time period. There are two kinds of regular wave theories, firstly, it is the linear wave theory applicable to waves with small amplitude and length and the Stokes second-order nonlinear theory applicable to waves of amplitude and length. According to McCormick (McCormick, 1976), the the existence of waves on a free surface, the reason is that the natural tendency of fluids is to maintain balance. When objects fall into the tank, they will interfere and form surface waves. The subsequent movement on the surface is the result of gravity and tends to return the water to its position without interference. Because these waves are caused by gravity, therefore called gravitational wave. The second point of view comes from Dean and Dalrymple (1991), who believes that the action of wind causes free surface disturbance. Waves can occur in various sizes and shapes. that's why called surface wave.[11]

The simplest theory is linear theory (or airy wave or first-order Stokes wave). The surface of the water is a cosine wave. Because the peak amplitude is the same as the trough amplitude, it is a symmetrical wave. The surface height is expressed by:

$$\eta = \frac{H}{2}\cos(\theta)$$

Then, using an appropriate theory, derive the particle velocity under the water wave based on the characteristics of the free surface (wave period T, wave height H, water depth d). Starting from zero velocity in the water, the gradient of the velocity field in the water can be observed. [6] Summarized the formulas of the horizontal and vertical components under the action of unidirectional waves. Horizontal velocity is showed by:

$$\mathrm{u} = \frac{\pi H}{T}\frac{\cosh(k(z+d))}{\sinh(kh)}\cos(\theta)$$

The vertical velocity is showed by:

$$v = \frac{\pi H}{T} \frac{\sinh(k(z+d))}{\sinh(kh)} \sin(\theta)$$

3.3.1 Analysis on the experimental data of regular waves

In this experiment, under intermediate and deep water conditions, the test case covers a wide non-linear range. Eleven regular waves are tested in order to verify the experimental setup. They are divided into two groups according to different wave periods T and wave steepness. The period of the first set of waves is 1.53s, and the period of the second set of waves is 0.94s. The test facilities for wave absorption and repeatability are also evaluated during the experiment to ensure the reliability of the experimental data. Because of the waves in the experiment cabin are essential to reproduce open ocean conditions and ensure consistent wave forms during the experiment.And the absorption efficiency directly affects the consistency of the waveform within several cycles. Then the repeatability of tank was assessed within a run and between independent runs. The free surface elevation measured at WP3 in the steady state query window is analyzed as well. The wave kinematics of regular waves are analyzed, which presented the free surface elevation measured by WP3 is compared with the theoretical elevation of the second-order Stokes theory.
In this experiment, different regular waves were tested to verify the experimental setup. Through the analysis of the experimental data of the tested regular waves, the following conclusions can be learned: First, when the experimental wave tank generates waves of different heights and steepnesses, the experimental elevation usually matches the relevant Stokes theory, just had a small mismatch in the shape of the wave. It can be noticed that for the frequency group of f=1.069 Hz (corresponding to deep water waves), the agreement between experimental elevation and theory is better. This is true for both wave amplitude and wave phase. There does not seem to be a relationship between the accuracy of the result and the non-linearity of the wave. The wave speed does not affect the consistency within each frequency group.
And, the measured speed value is compared with the theoretical value. For the velocity profile under the wave crest, the error is considered to increase as the wave non-linearity in each frequency group. For intermediate water waves, especially for trough velocities, the absolute horizontal velocity under the crests and troughs is underestimated. The experimental device is reliable for the tested deep-water short wave, and the error of its free surface height is within ±5%, and the error of particle velocity is within ±10%. As far as the peak period is concerned, the tested focused wave is closer to the short wave group than the long wave group. Therefore, the experimental measurement of the targeted focused wave is considered trustworthy.[6]

3.4 Focused waves

Focused waves are a special kind of water waves, which are different from regular waves or stochastic waves, and have a single large peak when they occur. On the basis of the research on the triggering mechanism of focused waves, many reasons for the generation of focused waves have been determined, such as temporal and spatial focusing of transient waves, wave-current interaction, geometric focusing caused by seabed topography, atmospheric forcing, nonlinear self-focusing Wait. If the wave height of a focused wave exceeds 2 to 2.2 times its effective wave height, it is usually defined as a weird wave or a rogue wave. therefore, Focused waves are often used in laboratories to simulate bizarre wave events observed under extreme sea conditions in order to better understand the generation process, the mechanism of these extreme waves and the hydrodynamic loads on floating or fixed ocean structures in the sea under the extreme ocean environments.[12]

3.4.1 Analysis on the experimental data of focused waves

In the experiment, eight different focused waves were tested in this study. For the focused waves, all waves have the same peak wave period. The significant wave amplitudes vary from 0.038m to 0.062m. The time evolution of the focused wave along the tank is shown in Figure 11. Remaining plots of free surface elevations at WP5-8 from experiment data, presented in Appendix A1. It illustrates the phenomenon of wave focusing in time and space, because the shape of the focused wave only appears at WP3. So the focal point must coincide with WP3, otherwise the wave elevation measured never corresponds to a focused wave. Therefore, the repeatability of the tank needs to be assessed again, for the generation of focused waves, making sure that the focal point is at WP3. Therefore, the focus must be consistent with WP3, otherwise the measured wave height will never correspond to the focused wave. Therefore, it is necessary to evaluate the repeatability of the tank again to generate the focused wave and ensure that the focus point is at WP3. Ten different runs were run in the experiment, and all the runs gave similar results, which means that the experimental tank showed good repeatability for generating focused waves.[6]

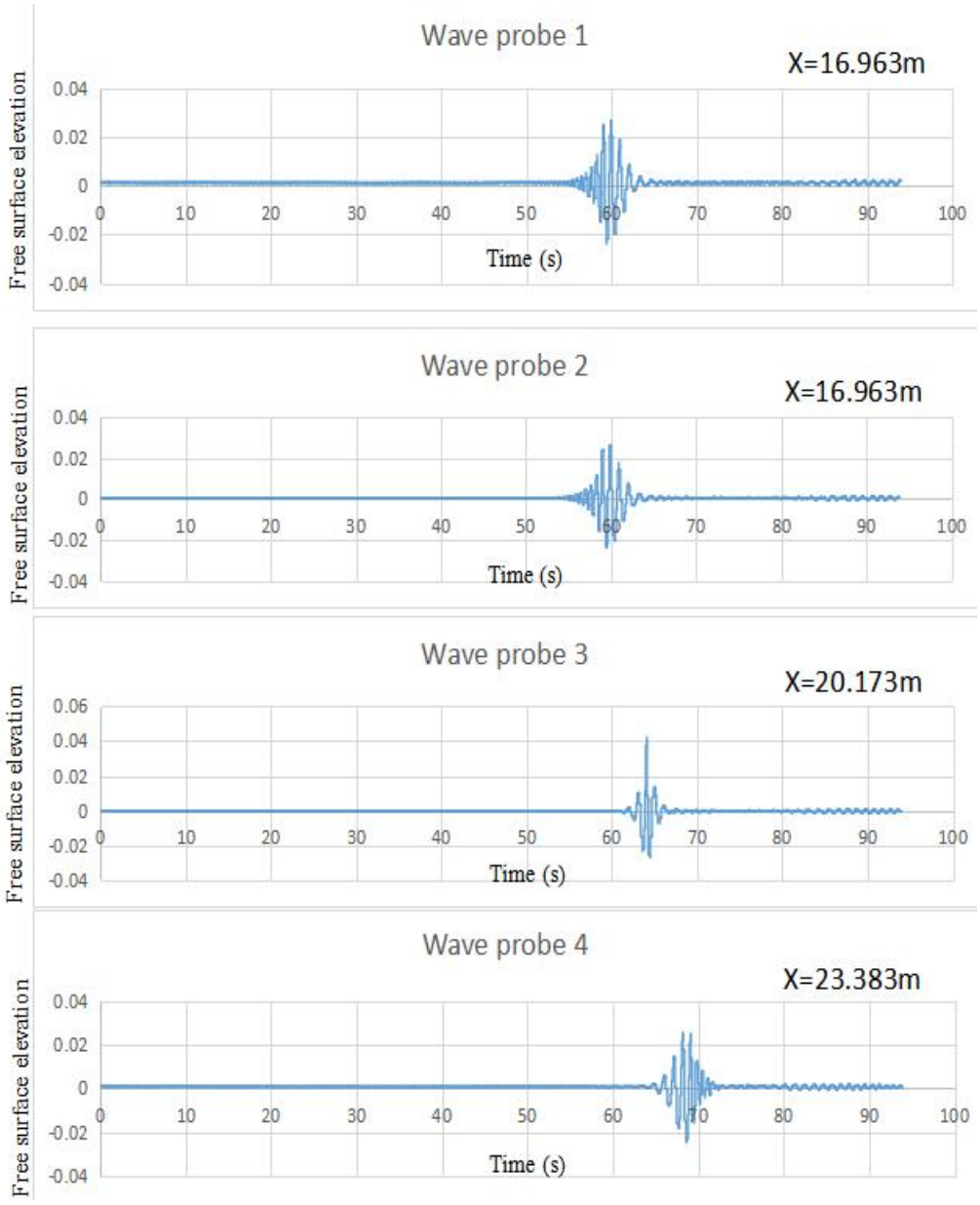

Fig.11: Time trace of a focused wave at four different locations along the tank

According to the analysis of the experimental results, we take the result of WP3 as the analysis case. The experimental results are shown in the Fig.12. The maximum displacement in the figure is about 0.014m and the period is 1, so we use a function with an amplitude of 0.014 m and a period of 1s as the input velocity of the regular wave.

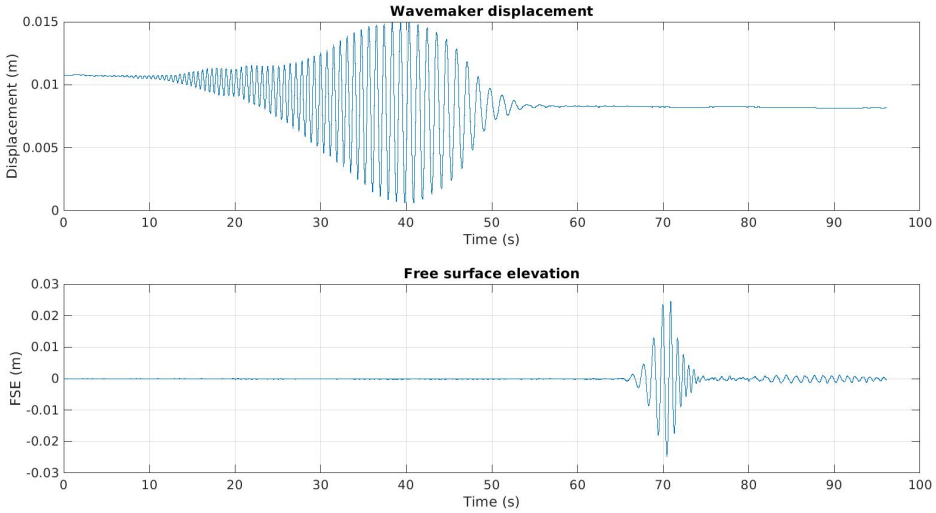

Fig.12: The experimental result of focused wave

4 ANSYS NWT

In this chapter, the tank geometry and wave gauges are detailed first section (in section 4.1). After it, the turbulence modelling are detailed in section 4.2. Then, meshing and wave maker will be explained in section 4.3 and section 4.4, respectively. At the end of this chapter, section 4.5 and section 4.6 are containing the temporal discretization and the simulation settings, respectively.

4.1 Numerical wave tank setup

4.1.1 Tank geometry

The geometry of the wave tank is shown on the Figure 13. Based on the study case, the length of the two-dimensional numerical water tank is 35 [m], the height of the tank is set to H_{tank} = 1 [m], the water depth is set equal to H_{water} = 0.7 [m] (with orange).

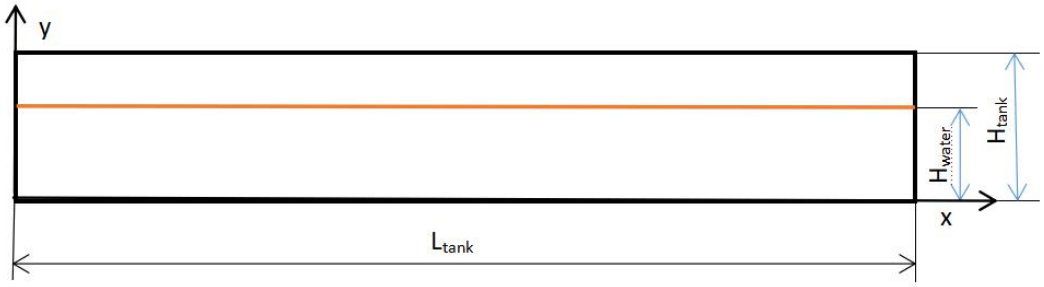

Fig.13: The geometry of the wave tank

4.1.2 Wave tank BCs

In order to get simulation results it is necessary to specify the information on the flow variables at the domain boundaries. It is important to define these correctly as they can have a significant impact on the numerical solution.The bottom of the tank and the wall of the left-hand side are set as wall boundaries in order to bound the domain. Tangential and normal fluid velocities are set to zero for the cells adjacent to the wall boundaries. In order to take the atmosphere above the free surface, the top of wave tank is set as a pressure inlet when simulating the movement of the free surface in the water tank. The interior of the domain is set to fluid and laminar zone. Fluid material input is set to air and water.

A moving wall has been used to as a velocity inlet. Although it is ideally intended for incompressible flows it is used here to input the flow of water only and does not include air within the prescribed flow conditions. The moving wall as a wave maker in the numerical wave tank. The velocity inputs required are the magnitude for each of the velocity components. Based on the experiment data, we make a velocity file to as a velocity of the moving wall. In Fig.14 the BCs of wave tank is shown schematically.

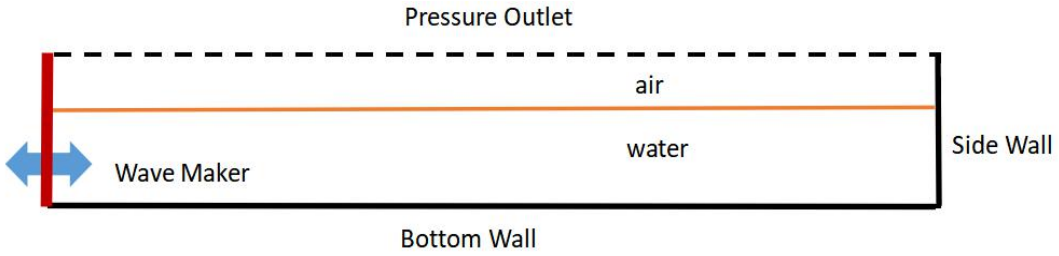

Fig.14: The BCs of wave tank

4.1.3 Wave gauges

In order to detect the heights of water waves over time in the wave tank, we were defined 8 lines (representing 8 wave probes in the experiment), where numerical wave gauges were situated to accomplish the measurements. These are respectively 16.963 [m], 20.173 [m], 23.383 [m], 23.519 [m], 23.723 [m], 24.044 [m] and 24.526[m] far from the moving wall. Figure 15 shows the lines across the simulation zone with yellow, the boundaries of the tank are marked with the line of black color.

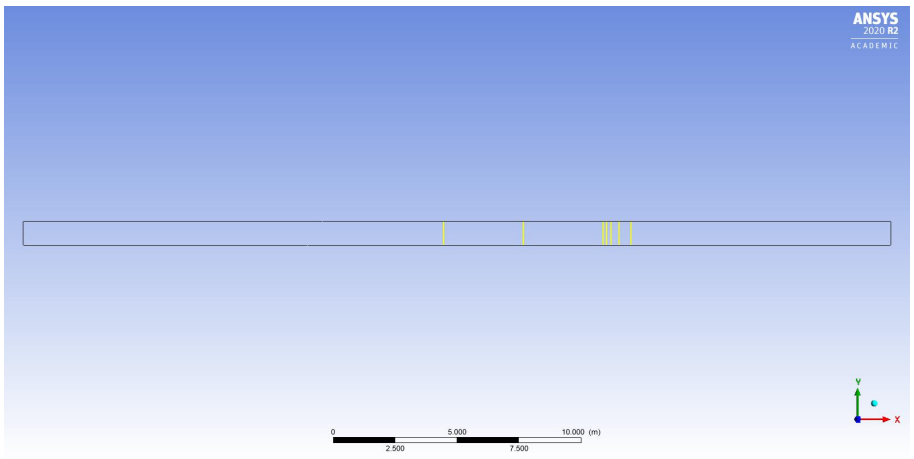

Fig.15: Defined 8 lines

Then the iso-clips are used to set up the numerical wave gauges. Based on the VOF model, the setup of the iso-clips applied in the simulation. However, this tank is quiet long, so in order to show their location more clearly, zoom in the area where they are located. Figure 16 shows the lines across the simulation zone with red, The specific location distribution of wave probes from moving wall are shown in Table 2.

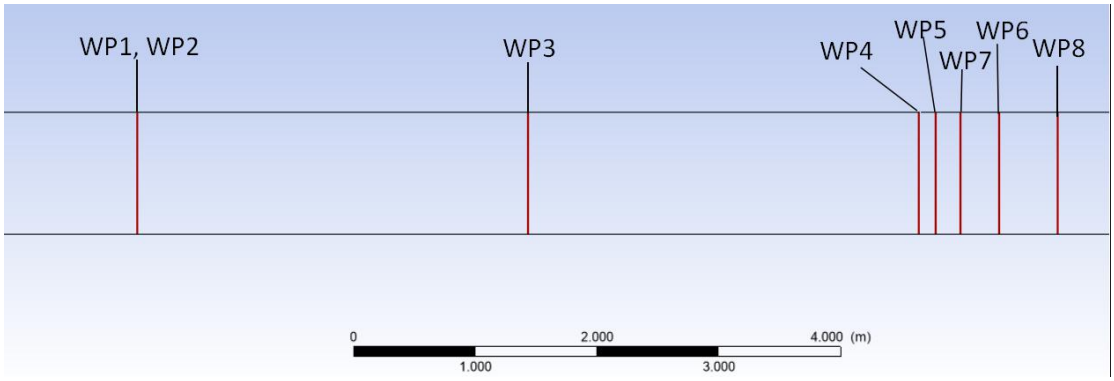

Fig.16: Wave probes

Table 2: The specific location distribution of wave probes

Wave probes 1–8 distances from moving wall [m]						
WP1	WP2	WP3	WP5	WP6	WP7	WP8
16.963	16.963	20.173	23.383	23.519	24.044	24.526

4.1.4 Dynamic mesh method

There are three mesh update algorithms for dynamic meshes in Fluent software: Smoothing, Layering and Remeshing.

4.1.4.1 Smoothing

Smoothing uses the displacement changes of the boundary nodes to adjust the node displacements in the fluid domain, and smoothly adjusts the grids, but the grids are still connected. This method assumes that the connecting line between the nodes becomes a spring. Due to the boundary motion, the displacement of the boundary node changes, and the spring line connected to the boundary node will generate a corresponding force. The force is proportional to the displacement. HooKe's Law is calculated, which causes the displacement to propagate along the fluid domain. According to Hooke's law and the principle of force balance, the resultant force on each node is zero, and the position of the grid node will change. Under normal circumstances, the spring deformation method can be applied to meshes of any shape, but for three-dimensional non-tetrahedral meshes or two-dimensional non-triangular meshes, the application of spring deformation method must meet two conditions: first of all ,the moving direction of the boundary is a single direction; the other hand, the moving direction is perpendicular to the boundary. If it is not satisfied, it may cause serious distortion of the grid.

4.1.4.2 Layering

The layering is generally applied to three-dimensional wedge-shaped grids or two-dimensional quadrilateral grids. The central idea is to reduce or increase the grid

according to the height change of the grid layer adjacent to the dynamic boundary Grid layer, that is, when the grid height is reduced to a certain range when the boundary is moving, the two adjacent grid layers will be merged into one layer; when the grid height is increased to a certain range, the adjacent grid layer will be decomposed two layers.
Layering has two split grid layer methods: Constant Height and Constant Ratio. Using the constant height method, the height of the grid division is the same; using the constant value ratio method, the result of the grid division is the grid of proportions.

4.1.4.3 Remeshing

Remeshing is used to reconstruct the mesh when the dynamic boundary displacement is larger than the element mesh size. It overcomes the disadvantages of using the spring deformation method to make the mesh quality poor, appearing negative volume, and the result does not converge. . In FLUENT, for the grids that are too large or too small, the size changes drastically, etc., the local mesh reconstruction method is generally used to re-divide the mesh. It can debug the volume mesh and the surface at the boundary. grid. There are some limitations when using the remeshing method: Only applicable to tetrahedral mesh (3D) and triangular mesh (2D); the surface mesh on the moving boundary is a triangular mesh (three-dimensional) or a linear linear segment (two-dimensional); the surface mesh to be repartitioned should be near the moving mesh node. the surface mesh is required to form a loop in the same plane.
The dynamic mesh model is automatically generated by FLUENT. If the simulation structure contains a dynamic boundary, FLUENT selects the dynamic mesh model according to the mesh shape around the dynamic boundary. If the surrounding mesh of the moving boundary is tetrahedron (3D) or triangle (2D), FLUENT dynamic mesh model selects spring deformation method and local mesh reconstruction method for mesh debugging;
If the surrounding mesh of the moving boundary is prismatic (3D) or quadrilateral (2D), the FLUENT moving mesh model selects the dynamic layer model for mesh debugging.

4.2 Turbulence modelling

4.2.1 DNS method

The first method is the so-called direct numerical simulation method (DNS method), which directly solves the N-S equation of turbulent motion to obtain the instantaneous flow field of turbulence, that is, random motion of various scales. All information about turbulence. With the development of modern computers and the research of advanced numerical methods, the DNS method has become a practical method to solve turbulence. However, due to the constraints of computer conditions, it can only be limited to some simple flows with low Re numbers and cannot be used in engineering applications. The direct numerical simulation of turbulence currently being done internationally is still limited to low demand numbers (Re～200) and

very simple flow shapes, such as flat plate boundary layer, fully developed channel flow, and back-step flow. Using direct numerical simulation methods to deal with complex flow problems in engineering, even the most advanced computer currently is still three orders of magnitude away.

4.2.2 LES method

The other method is called the large eddy simulation method (LES method). This is a compromise method that directly simulates the pulsation part of the turbulence, and averages (or is called filtering) the N-S equation in a small spatial domain, so as to remove small-scale vortices from the flow field and derive large-scale vortices. Satisfies the equation. The influence of the small vortex on the large vortex will appear in the large vortex equation, and then a model (sub-lattice scale model) is established to simulate the influence of the small vortex. Since the large eddy structure of turbulence strongly depends on the boundary shape and boundary conditions of the flow field, it is difficult to find a general turbulence model to describe the large eddy structure with different boundary characteristics, and direct simulation should be done. On the contrary, small-scale vortices have no direct dependence on boundary conditions, and generally have isotropic properties. Therefore, the sub-lattice model has greater universality and is easier to construct. This is its advantage over the Renault average method. Since first gave the LES calculation with engineering significance in 1970, the LES method has become one of the most powerful tools for calculating turbulence, and the application direction is gradually expanding, but it is still limited by computer conditions. It still has a long way to go to become a mature method to solve a large number of engineering problems.

4.2.3 RANS

Reynolds average simulation (RANS) is the application of statistical theory of turbulence, which averages the unsteady N-S equations over time to solve the time-average quantity required in engineering. The so-called turbulence model theory is to make various assumptions about Reynolds stress based on theoretical knowledge of turbulence, experimental data or direct numerical simulation results, that is, to assume various empirical and semi-empirical constitutive relationships, so as to make the average Reynolds equation of turbulence closed.
If turbulent flow needs to be modeled in the NWT, there are various appropriate methods and approaches, which can be distinguished by the accuracy and computational burden. DNS method can capture the turbulent fluctuation the most accurate way. By this approach, due to the scale of the fine turbulent eddies, a very accurate temporal and spatial discretization is required. This is greatly increasing the computational burden, which makes the DNS infeasible for practical applications in some cases.

Due to the modelling rather resolving these fine turbulent eddies, a method with lower computational requirements is reachable. Although, the fidelity of the solution by the LES simulation is lower, than the DNS, it is still a very accurate approach. LES is modelling the effect of the finer turbulent eddies and directly solves only the larger ones.
RANS and turbulence models If a model with lower computational cost is required, the RANS equations coupled with turbulence models are considerable. By this approach, the turbulence effects are considered as three-dimensional fluctuations of flow quantities. The result of the Reynolds decomposition is that the occurring fluctuations of the flow quantity.

4.2.4 Turbulence models

4.2.4.1 The Spalart-Allmaras Model

Spalart-Allmaras is a low-cost RANS model solving a transport equation for a modified eddy viscosity. When in modified form, the eddy viscosity is easy to resolve near the wall. Mainly intended for aerodynamic or turbomachinery applications with mild separation, such as supersonic or transonic flows over airfoils, boundary-layer flows, etc. Embodies a relatively new class of one-equation models where it is not necessary to calculate a length scale related to the local shear layer thickness. Designed specifically for aerospace applications involving wall-bounded flows. It has been shown to give good results for boundary layers subjected to adverse pressure gradients and gaining popularity for turbomachinery applications. This model is still relatively new.there is no claim is made regarding its applicability to all types of complex engineering flows and it cannot be relied upon to predict the decay of homogeneous, isotropic turbulence.

4.2.4.2 Standard k–ε model (SKE)

For the standard k–ε model (SKE), it is the most widely-used engineering turbulence model for industrial applications. It has such advantages robust and reasonably accurate, And contains submodels for compressibility, buoyancy, combustion, etc. However, it has some limitations when it is used. The ε equation contains a term which cannot be calculated at the wall. Therefore, wall functions must be used.
Generally performs poorly for flows with strong separation, large streamline curvature, and large pressure gradient.

4.2.4.3 Renormalization group k–ε model (RNG)

In the k–ε equations constants are derived using renormalization group theory. In this modle, it contains the following submodels: differential viscosity model to account for low Re effects; analytically derived algebraic formula for turbulent Prandtl or Schmidt number and swirl modification. But performs better than SKE for more complex shear flows, and flows with high strain rates, swirl, and separation.

4.2.4.4 Realizable k–ω model (RKE)

The term realizable means that the model satisfies certain mathematical constraints on the Reynolds stresses, consistent with the physics of turbulent flows. For Reynolds shear stresses: Neither the standard k–ε model nor the RNG k–ε model is realizable. This model has the following advantages: more accurately predicts the spreading rate of both planar and round jets. Also likely to provide superior performance for flows involving rotation, boundary layers under strong adverse pressure gradients, separation, and recirculation.

4.2.4.5 Standard k–ω model (SST)

The SST k–ω model uses a blending function to gradually transition from the standard k–ω model near the wall to a high Reynolds number version of the k–ε model in the outer portion of the boundary layer. It contains a modified turbulent viscosity formulation to account for the transport effects of the principal turbulent shear stress.
The model equations do not contain terms which are undefined at the wall, i.e. they can be integrated to the wall without using wall functions. This model accurate and robust for a wide range of boundary layer flows with pressure gradient. However, the treatment of far wall regions is more accurate by the k − ε model.

Based on theory of the Turbulence modelling, accomplished a comparison of these models through simulations. According to the results, it was clearly that the k–ω RKE model provides more accurate solution with slightly higher computational cost than the other model. Hence, the k–ω RKE turbulence model was applied in the research.

4.3 Meshing

To accomplish a comprehensive mesh convergence study, 4 different cases were defined with the same tank geometry, but differing meshes. As the Figure 17 shown, there are 3 horizontal regions across the length of the simulation zone of the tank. The free surface of the water is in the middle region, which starts 0.7 [m] from the bottom of the tank, and has a height of 10 [cm]. Underneath the middle region, there is the water region. At the top of the tank, there is the air region, with 0.2 [m] height.

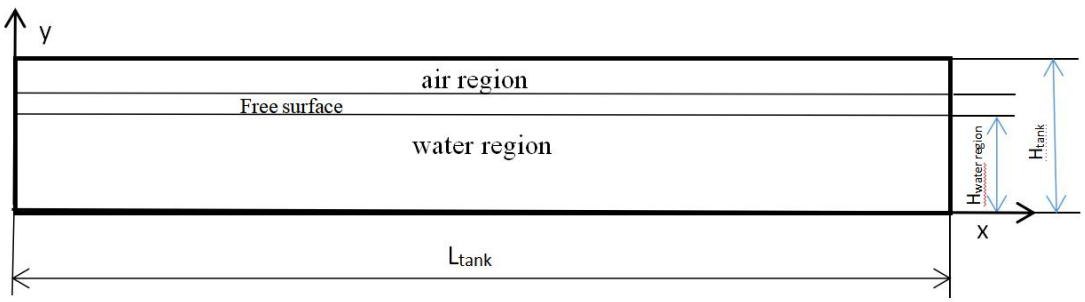

Fig.17: The 3 region of the tank

When dividing the mesh, since the free surface is the interface of the gas-liquid two-phase flow, the physical quantities in its vicinity vary greatly, so the mesh at the free surface should be refined. At the same time, the grid size near the interface between water region and air region must be similar with the grid size of the free surface in the horizontal direction. According to the calculated results, the size of the grid has a great influence on the accuracy of the results.

In the first case, the regions contain from the bottom to the top vertically 25, 10, and 12 cells, respectively. Horizontally, there are at least 10 cells per wavelength, as we knew, wavelength is 1.551[m] from the experiment data, which means the size of mesh at least 0.01551[m] in length. According to the length of wave tank is 35 [m], so we keep the size of cell is 0.014[m] in horizontal direction(equal at Δx in the Table3). These cell numbers are increased by 10,30,30,20 from case to case respectively, so in the last case there are 100, 30, 70 cells in the vertical regions.Because we must ensure that there are at least ten grids for each wave height in the vertical direction. The interface region has a height of 0.1 m, from the still water level to the boundary of air region, and meshed vertically with uniform cells of height $\Delta y = 0.001\,\text{m}$. At the same time, we have to note that only cells in the middle regions are increased. The number of cells in the other region are dependent from the number of cells in the middle region. These values are summarized in Table 3.

Table 3： Number of cells in every region of the simulation zone

Number of the case	Number of cells in the middle region Δy	Number of cells in the air region	Number of Cells in the water region	Horizontal cell height Δx	Maximum aspect ratio of free surface cell height $\Delta x/\Delta y$	Total number of cells
1	10	12	25	0.014	1.4	117500
2	20	15	30	0.014	2.8	162500
3	50	20	45	0.014	7	287500
4	80	25	55	0.014	11.2	337500
5	100	30	70	0.014	14	500000

The Figure 18 shows the mesh of the last case with the 3 vertical regions.

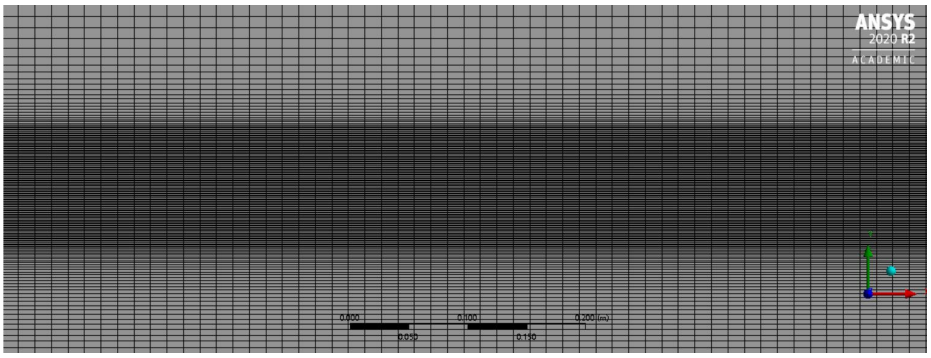

Fig.18: The mesh with the 3 region at the interface of the simulation

4.4 Wave maker

To provide accurate NWT simulations of OWCs, the generation of realistic waves is crucial. A number of techniques are available to generate waves in FLUENT.
This method consists in applying to the wave generator the boundary condition of mobile wall, which will move similarly to a piston. For this is used the dynamic mesh technique that allows to employ a variation of velocity to the mobile wall via a User Defined Function (UDF) or velocity profiles(Both of these two methods are detailed in section 4.4.1 and 4.4.2).
The movement control of the piston (mobile wall) is made according to the characteristics of the wave that will be generated, being necessary to know the period and the wave height of this wave. Then, using the transfer function, which relates the wave height and piston displacement, it is possible to determine the displacement that the piston needs to do to generate the wave with the desired characteristics.

4.4.1 User Defined Function(UDF) method

UDF (User-Defined Function), which is a user-defined function, is a function written by the user in C language and can be dynamically loaded by the fluid mechanics software FLUENT to improve the solution performance of the software. UDF is written by using DEFINE macros (provided by Fluent Inc.), which can use C language library functions or predefined macros, through which the data in FLUENT can be accessed. UDF to udf. The h header file is the initial statement, so that the DEFINE macro, FLUENT macro and other functions can be called during compilation. Whether it is the value passed from UDF or the value passed to the solver, or the value returned by the solver to UDF, it is the international system of units.
In FLUENT, define variables on the boundary with DEFINE_PROFILE(name, thread index) Where name is the variable name. When UDF is successfully compiled and connected in FLUENT, the variable name will be displayed and can be selected; thread is a pointer to the defined boundary; index determines the stored variable. For example, based on the data of experiment, the velocity of moving wall can be written

as a function: $v = 0.045\sin(2\pi t)$. The boundary position does not move and the speed is $v = 0.045\sin(2\pi t)$, so the corresponding UDF statement can be written as shown in the following figure 19.

```
#include" udf.h"
#define PI  3.1415926
DEFINE_PROFILE(inlet_x_velocity,thread,index)
{
real time;
Face_t f;
begin f loop(f,thread)
{
time=RP_Get_Real(" flow-time" );
F_PROFILE(f,thread,index)=;
}
end_f_ loop(f,thread)
}
```

Fig.19: The UDF file

Since most of UDF macros are contained in "udf.h", the statement must start with #include "udf.h". The boundary velocity defined above is an unsteady value and is related to the fluid motion time. The time statement defined in the UDF is "time=RP_Get_Real("flow-time")". In the program, begin f loop(f,thread) and end_f_ loop(f,thread) are combined into a loop structure for finding surface clues. It can query the entire surface of the boundary to be assigned and assign the speed value to the F_PROFILE. Under the inlet X velocity variable, this variable defines the corresponding boundary in FLUENT.

4.4.2 Velocity profile method

Profiles can be boundary conditions, cell zone conditions, and initial conditions for discrete phases. ANSYS Fluent provides a very flexible profile definition mechanism. This feature allows you to use experimental data, data calculated by an external program, or data written from a previous solution using the Write Profile Dialog Box (as described in Reading and Writing Profile Files) as the boundary condition for a variable.[13]

The following is a list of the six types of profiles that can be read into ANSYS Fluent, as well as information about the interpolation method employed by ANSYS Fluent for each type.

4.4.2.1 Point profiles

Point profiles are specified by an unordered set of points: for 2D problems or for 3D problems, where. Profiles written using the Write Profile dialog box and profiles of experimental data in random order are examples of point profiles.

ANSYS Fluent will interpolate the point cloud to obtain values at the boundary faces. The default interpolation method for the unstructured point data is zeroth order. That is, for each cell face at the boundary, the solver uses the value from the profile file located closest to the cell. Therefore, to get an accurate specification of an inlet profile using the default interpolation method, your profile file should contain a sufficiently high point density. For information about other available interpolation methods for point profiles.

4.4.2.2 Line profiles

Line profiles are specified for 2D problems by an ordered set of points: Zeroth-order interpolation is performed between the points. An example of a line profile is a profile of data obtained from an external program that calculates a boundary-layer profile.

4.4.2.3 Mesh profiles

Mesh profiles are specified for 3D problems by an by mesh of points: , where and . Zeroth-order interpolation is performed between the points. Examples of mesh profiles are profiles of data from a structured mesh solution and experimental data in a regular array.

Radial profiles are specified for 2D and 3D problems by an ordered set of points. The data in a radial profile are a function of radius only. Linear interpolation is performed between the points, which must be sorted in ascending order of the field. The axis for the cylindrical coordinate system is determined as follows:

- For 2D problems, it is the -direction vector through (0,0).
- For 2D axisymmetric problems, it is the-direction vector through (0,0).
- For 3D problems involving a swirling fan, it is the fan axis defined in the Fan Dialog Box (unless you are using local cylindrical coordinates at the boundary, as described below).
- For 3D problems without a swirling fan, it is the rotation axis of the adjacent fluid zone, as defined in the Fluid Dialog Box (unless you are using local cylindrical coordinates at the boundary, as described below).
- For 3D problems in which you are using local cylindrical coordinates to specify conditions at the boundary, it is the axis of the specified local coordinate system.

4.4.2.4 Axial profiles

Axial profiles are specified for 3D problems by an ordered set of points: , where . The data in an axial profile are a function of the axial direction. Linear interpolation is performed between the points, which must be sorted in ascending order of the field.

4.4.2.5 Transient profiles

Transient profiles are specified for 2D and 3D profiles by an ordered set of points: Linear interpolations are done between the points which must be sorted in ascending order of the (time or crank angle) field. Examples of transient profiles are transient cell zone and boundary conditions (see Defining Transient Cell Zone and Boundary Conditions) and point properties for particle injections (see Point Properties for Transient Injections).

We can use profiles to specify position, velocity, and angular velocity. There are two different valid profile formats for moving and deforming mesh cases.

You must use the appropriate variable nomenclature when writing your profile so that Fluent can properly interpret your inputs. For position, use x, y, and z. For specifying velocity, use v_x, v_y, and v_z. Similarly, for angular velocity, use omega_x, omega_y, and omega_z.

The velocity of the dynamic mesh file is as follows: For focused waves, the Figure 20 shown the velocity file of moving wall.

```
velocity_u 2 12019  0
time v_x
0           0
0.008       0
00.016      0
.     .
.     .
.     .
51.594      0
51.602      0
51.609      -0.0067525
51.617      0
51.625      0
51.633      0
51.641      -0.007715714
51.648      0
51.656      0
51.664      0
51.672      -0.0067525
51.680      0
51.688      0
51.695      0
51.703      -0.00675125.
.     .
.     .
.     .

93.883      0.0067525
93.891      0.0000874466
```

Fig.20: The velocity file of moving wall for focused wave

For regular waves, the Figure 21 shown the velocity file.

velocity_u 2 10001 0
time v_x

0	0
0.01	0.002761671
0.02	0.005512444
0.03	0.008241461
0.04	0.010937953
0.05	0.013591277
.	.
.	.
.	.
30.86	-0.033888942
30.87	-0.032061715
30.88	-0.030107954
30.89	-0.028035371
30.9	-0.025852146
30.91	-0.023566893
30.92	-0.021188633
30.93	-0.018726751
30.94	-0.016190963
.	.
.	.
.	.
99.97	-0.008241461
99.98	-0.005512444
99.99	-0.002761671
100	1.73E-16

Fig.21: The velocity file of moving wall for regular wave

4.5 Temporal discretization

The convergence condition of Courant–Friedrichs–Lewy is a necessary condition for convergence when calibrating some partial differential equations numerically. When it is used as a numerical solution, it appears in the numerical analysis of an explicit time integration scheme. Therefore, in many explicit time-travel computer simulations, the time step must be less than a certain time.[14]

Therefore, the CFL condition expresses that the distance that any information travels during the timestep length within the mesh must be lower than the distance between mesh elements. In other words, information from a given cell or mesh element must propagate only to its immediate neighbors. So it is necessary to know what the maximum time step is, then we can choose a suitable time step to run this simulation.[15]

In the two-dimensional case, the CFL condition has the following form:

$$C = \frac{u_x \Delta t}{\Delta x} + \frac{u_y \Delta t}{\Delta y} \leq C_{\max}$$

where the dimensionless number C is called the Courant number, u_x is the flow velocity in the x direction, u_y is the flow velocity in the y direction, Δt is the time step, Δx and Δy are the length intervals in x and y direction, respectively (cell length and height), and C_{max} is the upper limit of the Courant number. For any explicit simple linear convection problem, the Courant number must be equal or smaller than 1, otherwise, the numerical viscosity would be negative. The time step is appropriate, if the $C \leq 1$ inequality is fulfilled. When we choose the formulation of volume friction is explicit , where the default Courant number is equal at 0.25, the figure 22 shown the setup of multiphase model. so the adequate time step can be calculated with the previous equation.

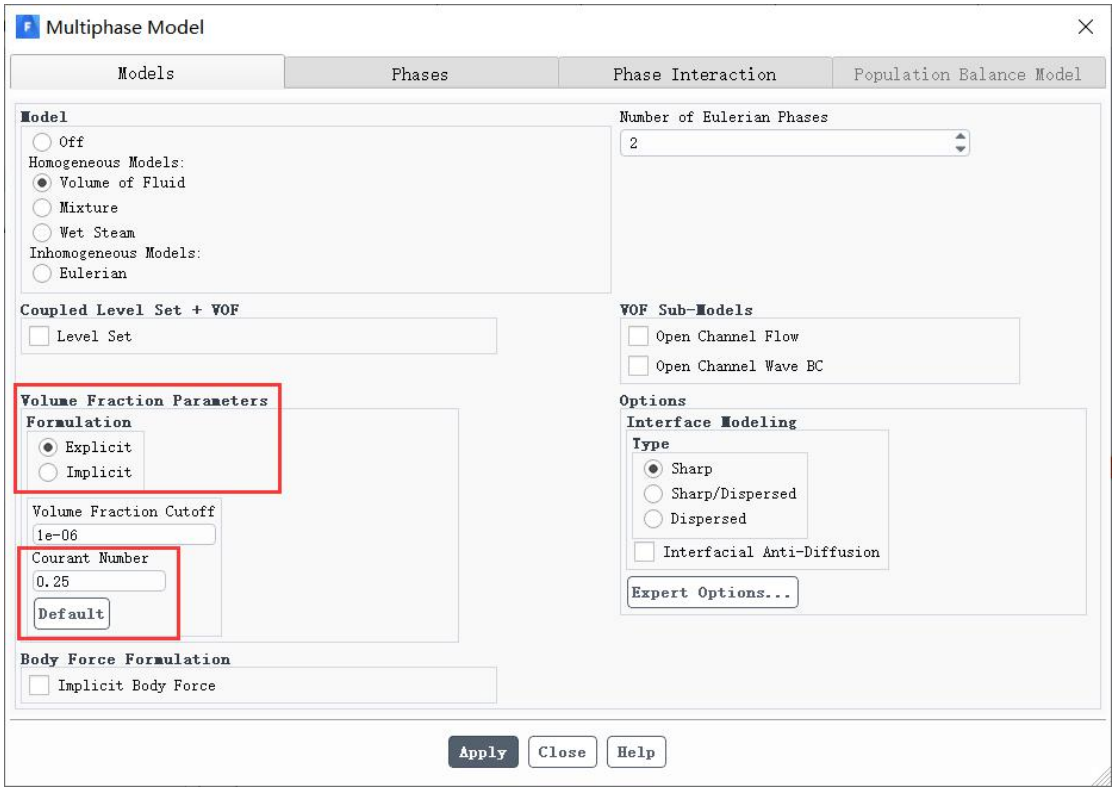

Fig.22: The setup of multiphase model

Based on the previous calculation of velocity. It is a maximum velocity at the surface, z=0, where

$$u = \frac{\pi \times H}{T} = \frac{\pi \times 0.02}{1} = 0.0628 ,$$

therefore, the maximum velocity occurs at the free surface (where the cells are the smallest) and equals 0.0628 m/s. The vertical and the horizontal velocities are the same, however the mesh is smaller in the vertical direction. Since we use at least 10 cells per wave height, we used 20 cells per wave height in the simulation, so this would give a cell size of 0.001m(Δy). So the maximum time step would need to be:

$$\Delta t \le \frac{\Delta y}{u_y} = \frac{0.001}{0.0628} = 0.016$$

So we choose the time step is 0.01s.

4.6 Simulation settings

In the FLUENT software, after reading the above grid file and velocity file, the basic parameters of the model setting as follows: the flow was assumed to be viscous, transient, and incompressible for the numerical model. So the solver chooses 2D, Unsteady. The two-phase flow was modeled through the VOF method, which can be only used with pressure-based solver. So choose the pressure based, and adopts laminar flow model; choose Volume of Fluid for two-phase flow model, the number of phases is set to 2, set air as the primary phase and water as the second phase; The pressure outlet boundary condition was applied for the top of the tank. So control conditions (Operating Condition) set a standard atmospheric pressure, that is, 101325Pa, select the effect of gravity, the acceleration direction is along the Y axis, and the value is. 9.81 N/ m^2, working density is 1.225kg/m^3.
In the setting of the method of solution, the pressure-velocity coupling selects the SIMPILE scheme, which is generally aimed at non-steady-state problems, and the total calculation efficiency is relatively high: in the discrete format, the pressure selects Body Force Weighted. The calculation time step is taken as 0.01s, and each time step is iterated 20 time. But note that this simulation setting was just used to running calculation for regular wave. About the simulation setting of the focused wave, it will be detailed in the 5.2 section.

5 Results

5.1 Single frequency

For regular wave, during the period of simulation, due to it needs the large amount of calculation workload for the simulation of the full size wave tank, in order to save time and avoid repeated experimental work, before simulating the full size wave tank, we made two shorter tanks as test cases, 5 m and 10 m wave tank, respectively. Then observing the wave height elevations to ensure that the correct waves are generated. In order to realize the detection of wave height fluctuations, a wave probe is set every 1 meter in the numerical water tank. After that, keep the same setting in the FLUENT, the simulation is performed on the entire size of the tank.
The reliability, accuracy, and applicability of the numerical flume can be evaluated by analyzing the time evolution of the instantaneous wave surface, the time history analysis of the wave amplitude at a certain position, and the wave surface shape analysis at a certain moment. Here we take the test case of 10 meter wave tank as a example, the time evolution of the regular wave surface was analyzed. Figure 23 shows the diachronic evolution of the regular wave numerical generation process.

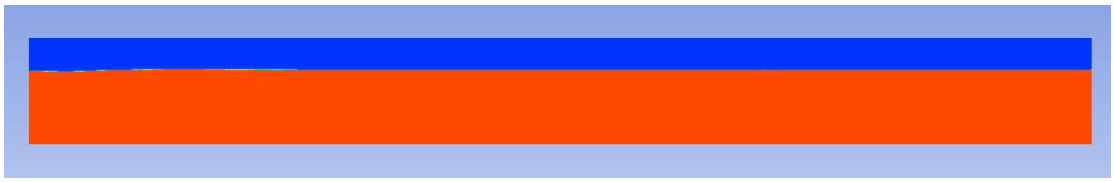

T=1 s

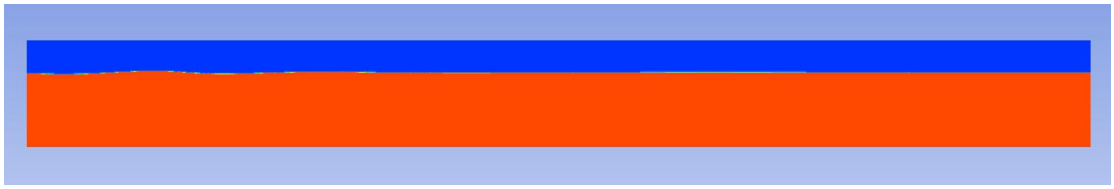

T=3 s

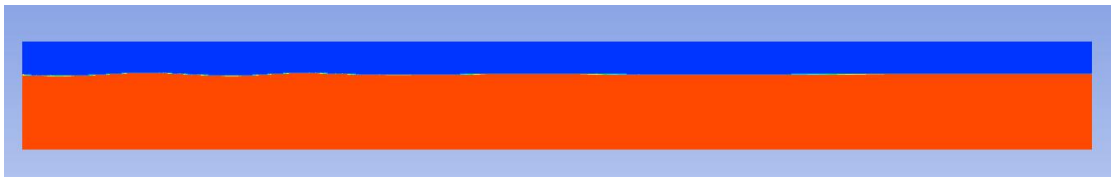

T=5 s

T=7 s

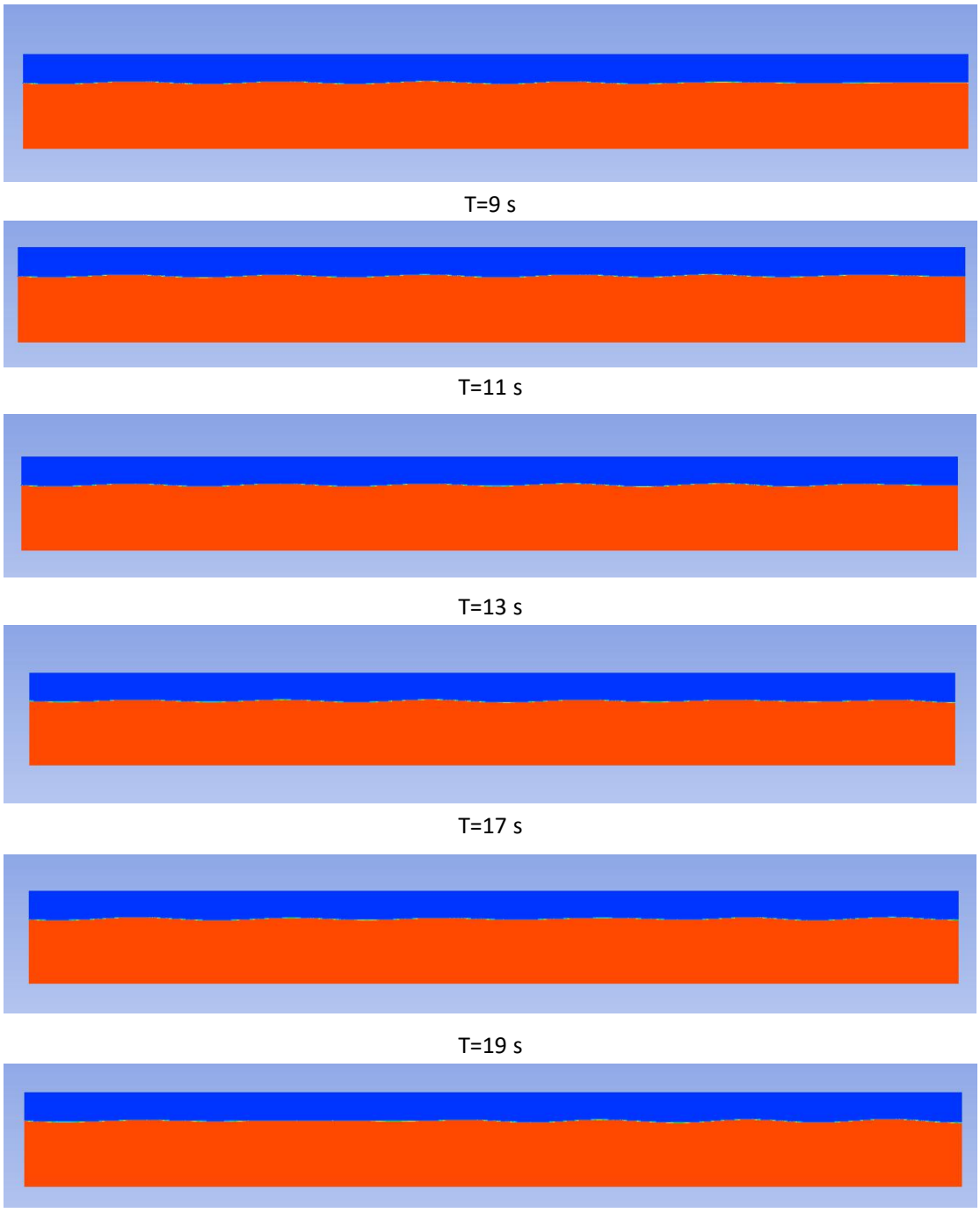

Fig.23: The diachronic evolution of the numerical generation of regular waves

The calculation results show that the shape of the generated regular wave is consistent with what we expect. When the wave-making time reaches 13.0s (T=13s), the wave-making process tends to be stable.

Then we have analyzed the monitoring results at the location of wave probe 1(at x=1 meter). Because the position of the wave probe 1 is close to the wave maker , it is less affected by reflection of the wall at the end of the wave tank. As showed in Figure 24

It can be observed that the steady state window of about five periods framed in red. The wave height and period of the regular wave are exactly what we expect.

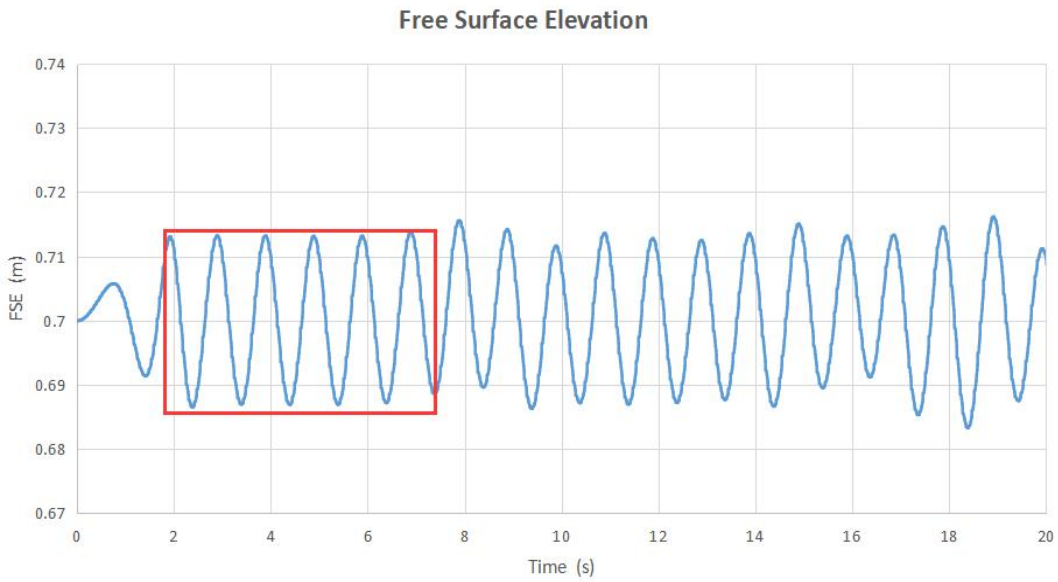

Fig.24: Complete time trace and steady state window at 1meter

Through the analysis of the simulation results of the short wave tank, we can know that the wave maker can produce the waves we expect, so we can start the simulation calculation for the full size wave tank.

In order to ensure that the fluctuation of the free surface wave is monitored, in addition to the eight wave probes set at the same position as the experiment, another 6 wave probes are set every 5 meters. In order to avoid numerical instability caused by sudden disturbance in the wave domain, the wave maker needs to be started slowly. As can be seen from Figure 25, in the range of t=15-20s, shows the complete time tracking of regular wave at the position of 5 meter , the steady-state window is about 10 periods with a black frame.

The wave surface shape is gentle and the wave is the most stability. The amplitude is about 0.014m, which shows that the disturbance of the whole area is small when the wave maker is started, and the expected control requirements are met. It can be clearly seen from the shape of wave surface elevation that the wave amplitude is increasing in the range of t=0-8s, which also shows that the wave from generate to stable need some time, verifies the starting process of the wave maker. With the increase of time, the free surface tends to be stable after t=15s, and the wave surface changes periodically with the amplitude 0.014 m. Within a wavelength range at the end of the tank, the wave surface has dropped slightly. This is due to reflection when the wave get the end of the tank.

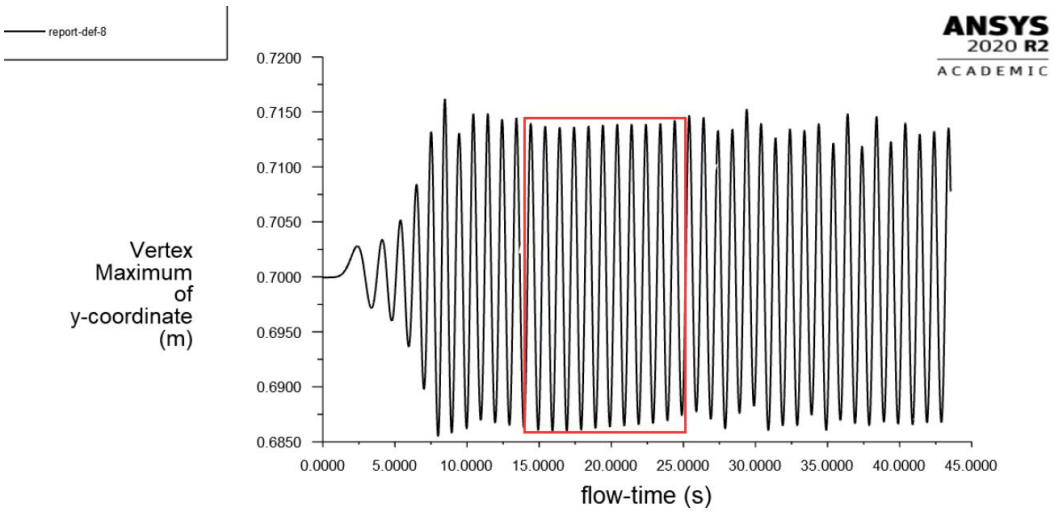

Fig.25: Complete time trace and steady state window for case

5.2 Focused wave

Generating focused waves in a numerical wave tank is more challenging and difficult than regular waves. Firstly, the speed of the focused wave is unknown because it is a polychromatic wave and each component propagates at a different speed. Therefore, in the process of running calculation, the time step is difficult to determine. As we discussed in the 4.5 section, we need to know the component of the speed on the direction of y axis, and we can calculate the smallest time step when the Courant number is less or equal to 1. At the beginning of running calculation, an adaptive calculation method (shown in Figure 26) was used, but an error message appeared during the calculation process (The Courant number is greater than 250). Therefore, we must continuously adjust the time step to ensure the completion of the calculation. Unfortunately, after many adjustments, even if the time step is adjusted to the minimum value, the same error message will still appear. Therefore, we must adopt a fixed calculation type during the process of simulation.

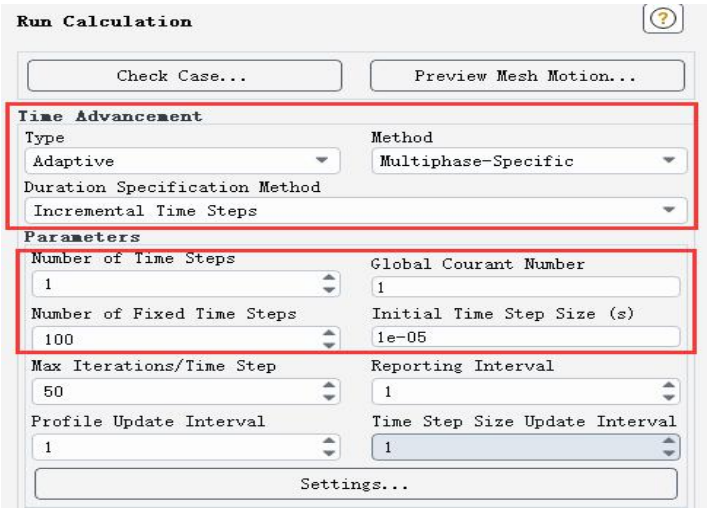

Fig.26: The adaptive type

Secondly, the distance between the wave maker and the wave probes that measures the free surface elevation is quite long, this will result in the need to spend a lot of time waiting for the results, and then make a comparison with the experimental data to verify the accuracy of the simulation. For example, the position of wave probe 8 is 24.526 m at the numerical wave tank. The focused wave will occur at about 75s based on the experiment data. So the total time of running calculation at least 75s. According to the previous experience, it takes at least two days to complete the calculation, so this simulation need a lot of time to wait for the correct result. To save time to get the results, we must the time step is maximized under the guaranteed completion of the calculation condition. After many tested, we found that a time step of 0.005 can produce a focused wave very well. The final calculation type and time step are shown in Figure 27.

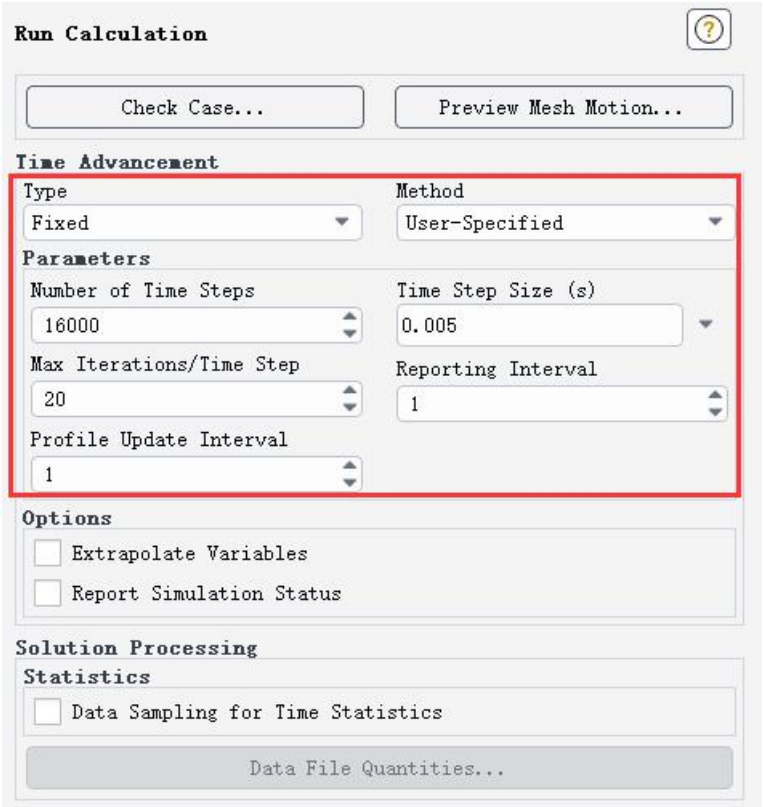

Fig.27: The fixed type

In order to ensure that the focused wave can be generated in the correct position, first of all, we can make a verification of the wave maker. When the calculation of simulation is done, we can got a plot of displacement for wave maker. So the numerical results of wave maker can be compared to experimental data. In order to have an intuitive comparison, the numerical results and experimental data are plotted together. The comparison result is shown in the Figure 28. From the Figure 28, it looks that the numerical and experiment amplitudes match well for the wave maker, which suggests that the moving wall sufficient to calibrate accurately the wave maker.

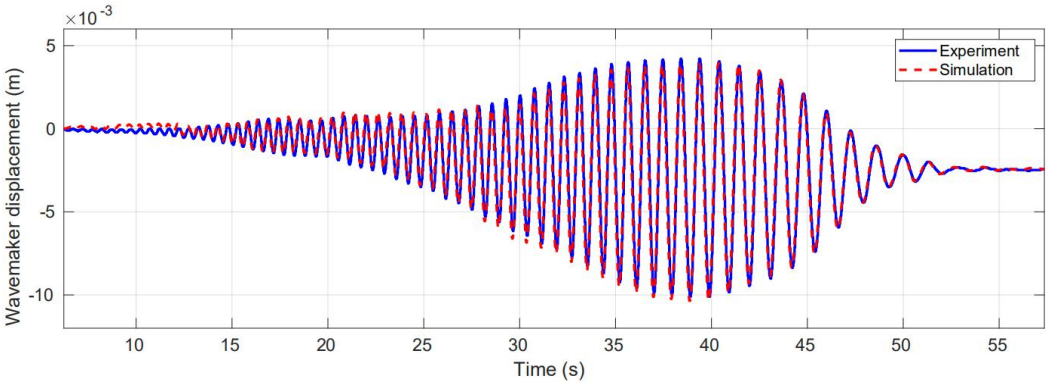

Fig.28: Comparison of numerical results and experimental data for wave maker

5.2.1 First test case

However, even though the wave maker has been checked, the numerical wave tank did not produce the focused wave at the expected location and height. When we run the simulation for focused wave, we keep the same setting with the regular wave. In the Multiphase model panel, we choose the explicit formulation in the volume fraction parameters, the setting of Multiphase model was shown in figure 26 with red rectangle. For the panel of viscous model, we choose the k–ε realizable turbulence model in this simulation(shown in Figure 29). Regarding the solution method, we keep the default in this panel. This simulation is considered the first test case.

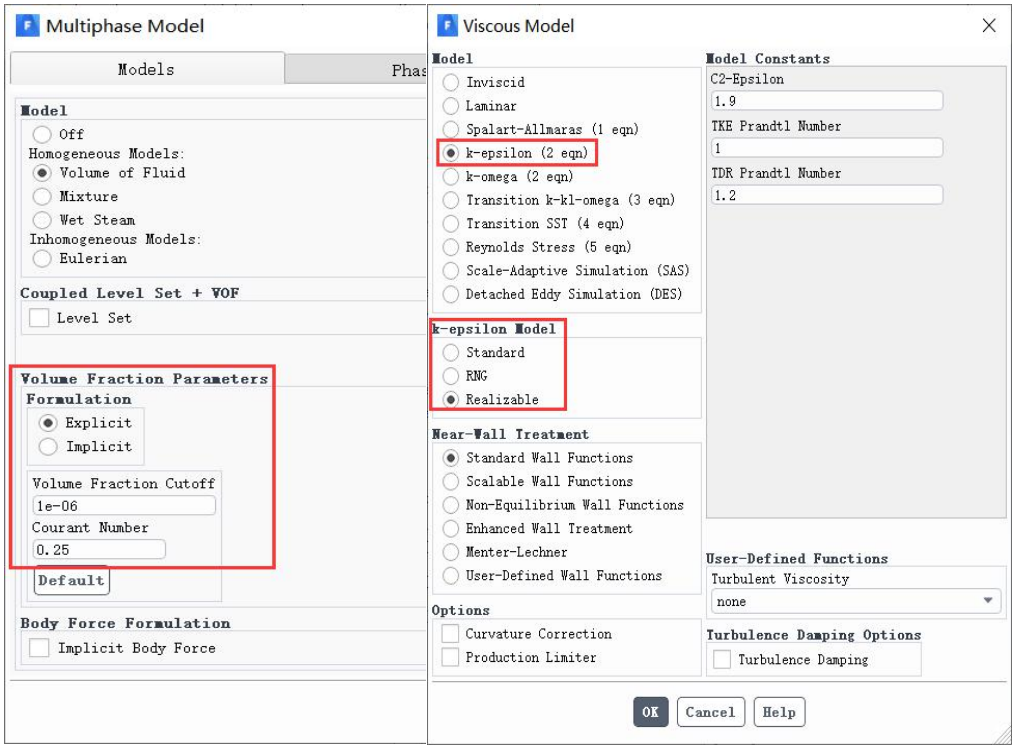

Fig.29: The setting of multiphase model and viscous model

When the calculation is completed, the data measured by the wave probe is processed. The time evolution of a focused wave along the numerical wave tank is shown in Figure 30. Remaining plots of free surface elevations at WP5-8 presented in Appendix A2. It looks well the phenomenon of wave focusing in time and space along with the tank.

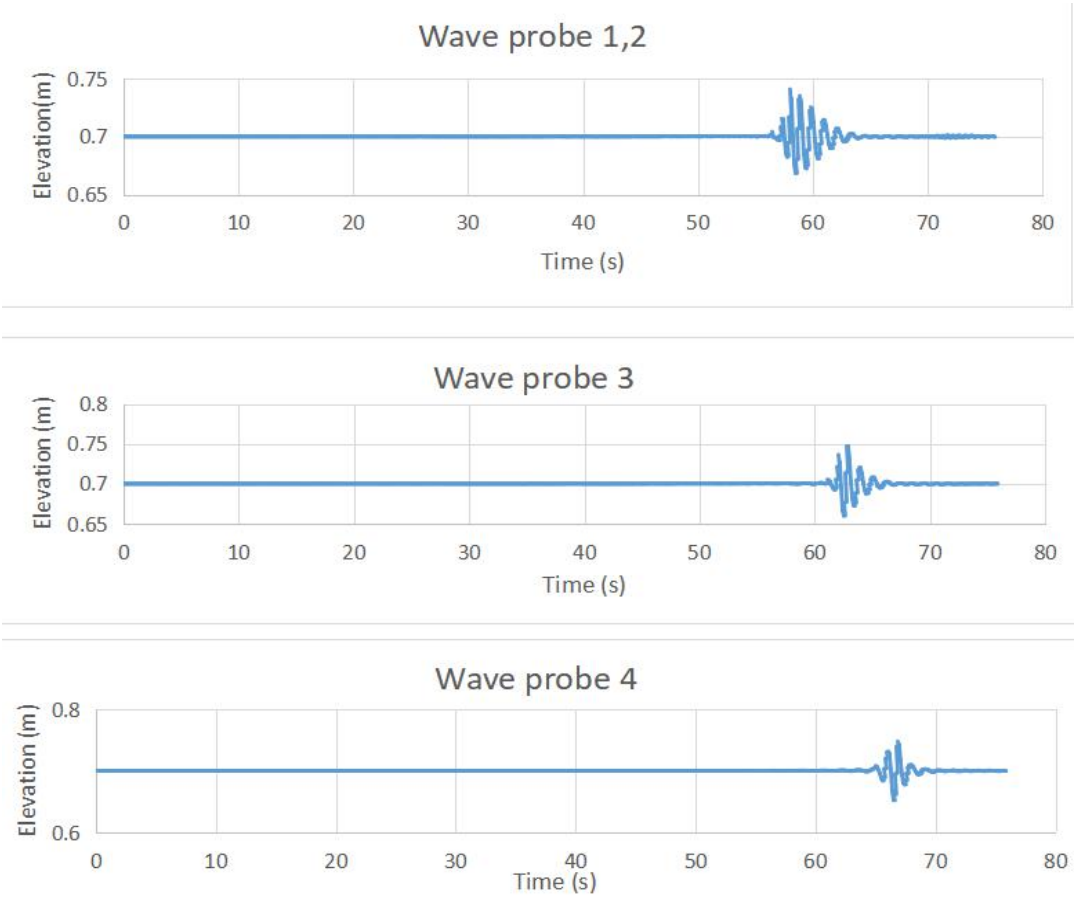

Fig.30: Time trace of a focused wave at three different locations

Based on the experiment data, we know that the shape of a focused wave only appears at WP3. And the focal point of the simulation result must coincide with the experiment result of WP3, otherwise the wave elevation measured never corresponds to a focused wave. Therefore, the experimental and simulation free surface elevations are compared for WP3. In order to generate the plot, the time interval was adjusted appropriately, because the time interval of the experimental data is not uniform, and the time interval of the simulation data is uniform. In order to make them coincide at the same time and have a clear contrast, so the time of the experimental data is divided equally. The comparison of experiment data and simulation result are presented in Figure 31.

From Figure 31, it can be found that the error between experiment and simulation is not so much in peak time, but there is a mismatch in height. It can be noticed that the elevation of the simulation is more than the crest of experiment. But the shape of wave is similar with experiment elevation. So some change in the setting of

simulation should be required.

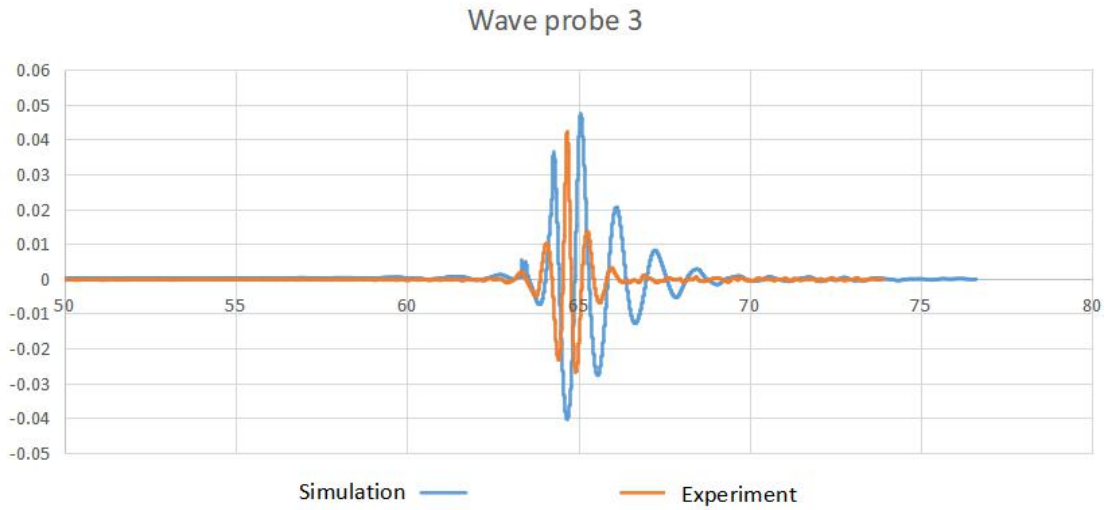

Fig.31: Comparison of simulation and experiment for WP3

The process of obtaining the frequency and amplitude of each wave component of the focused wave is to use the amplitude in the experimental spectrum analysis. So in order to better understand the origin of the difference between the experimental data and the simulation results, a spectrum analysis of the simulation signal was performed for WP3. As we know, the frequency and amplitude associated with each wave component of focused wave from the simulation time trace are directly derived from the fast Fourier transform (FFT) of the time trace. However, this job is difficult to calculation by hand, which was solved with Matlab. The plots was made by Dr Josh Davidson, during the period of my consultant. The wave elevation and its spectrum for WP3 is shown in Figure 32.

From the frequency spectra, as it can be seen, the frequencies is between 0Hz and 2.0Hz and correspond to the frequency limits of the experimental wave tank. And based on the experiment data, the energy densities of the frequency components should be 10^{-5} m^2/s. It can be noticed that the energy densities of the frequency components are smaller in the experimental result from the right plot in Figure 32.

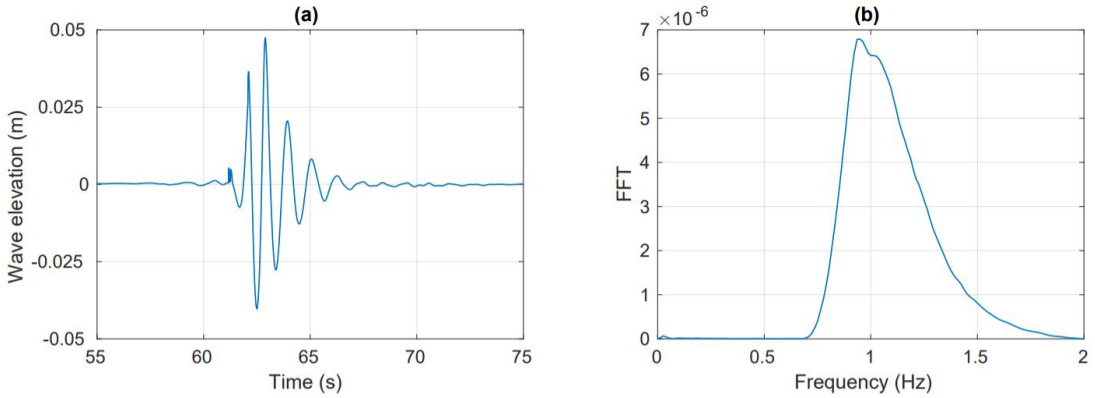

Fig. 32: The wave elevation and its spectrum for WP3

However, from the plots of simulation, It can be noticed that the WP4 have a better match with the experiment data, which is consistent with the observation of the elevation plot in the experiment in time and shape. So a spectrum analysis of the simulation signal was performed for WP4 as well. The wave elevation and its spectrum for WP4 is shown in Figure 33. From the frequency spectra, it can be observed that the energy densities of the frequency components more than the WP3, which is still smaller than the experiment result. For WP4 have a better match observed for the focused waves might be due to wave maker need take a certain amount of time to generate wave, so it effects the peak of free surface elevation happening during the time the wave travelled from the wave maker to wave probes. But it's just a speculative view, and further tests are needed to verify it.
Unfortunately, the larger mismatch observed for the focused waves, we can not determine the specific reason for this result based on the knowledge we have learned, so we can only try to change the settings to get better results based on the study of literature review, so in order to improve the result, we conducted a second test case. Details will be introduced in the following section.

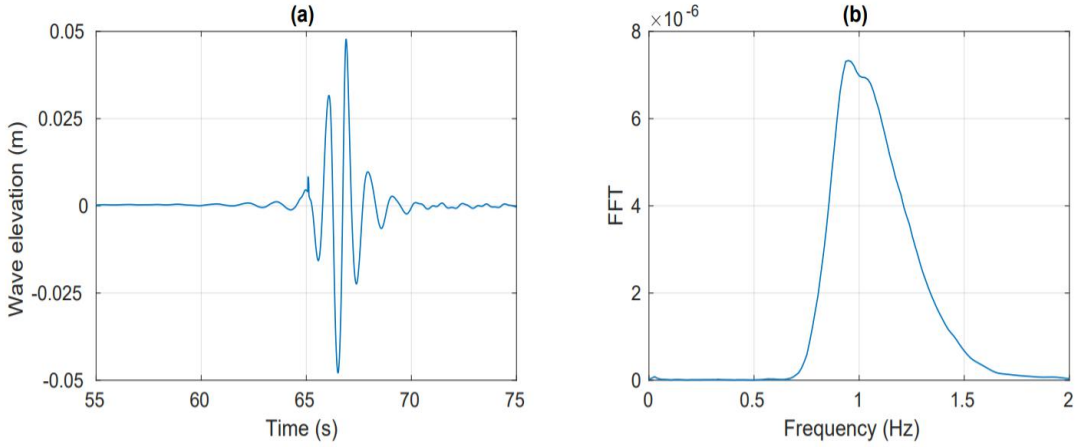

Fig. 33: The wave elevation and its spectrum for WP4

5.2.2 Second test case

Through the analysis of the results, we can know that the simulation elevation are higher than the experimental results at WP3. In order to obtain accurate results, try to change the simulation settings to get some good simulation results. This case will be as the second test case. In the multiphase model panel, we changed the explicit formulation to implicit formulation in the volume fraction parameters and enable the body implicit force, the setting of multiphase model was shown in Figure 26 with red rectangle. For the panel of viscous model, we changed the k–ε realizable turbulence model to k–ω SST model in this simulation. The detailed setting changes shown in Figure 34.

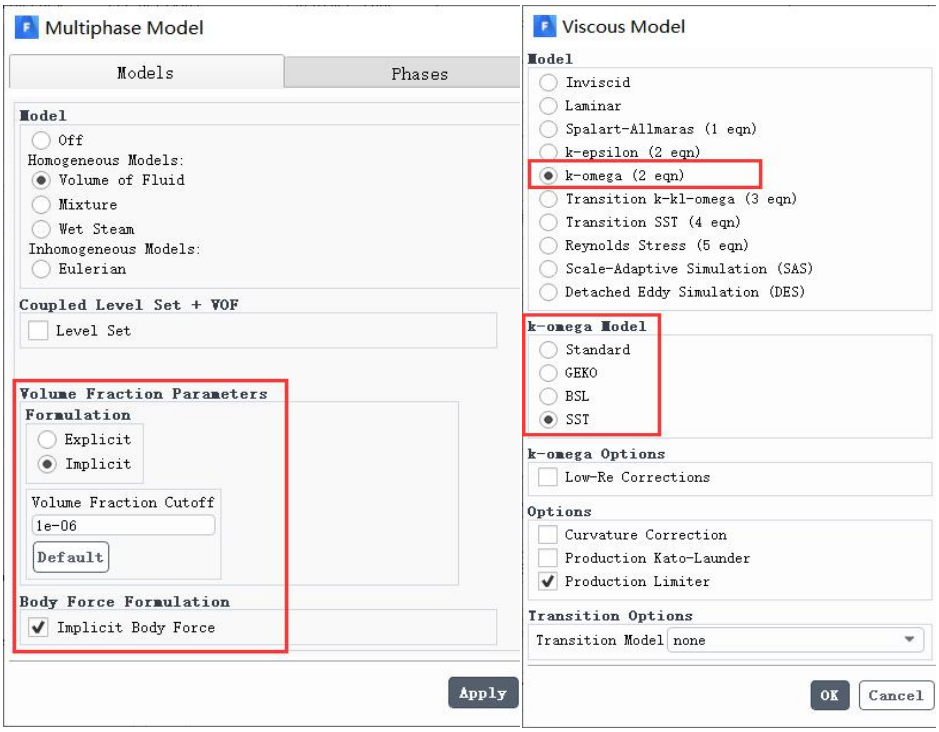

Fig.34: The setting of multiphase model and viscous model

Regarding the solution method, we change a lot in the part of spatial discretization, in order to get good simulation result, through literature survey, we adopt common solution methods for generating waves based on the previous researcher's experience. The pressure select body force weighted, momentum choose the first order upwind, and the second order upwind were used for the turbulent kinetic energy and the turbulent dissipation rate, the setting of solution methods shown in Figure 35 with red rectangle.

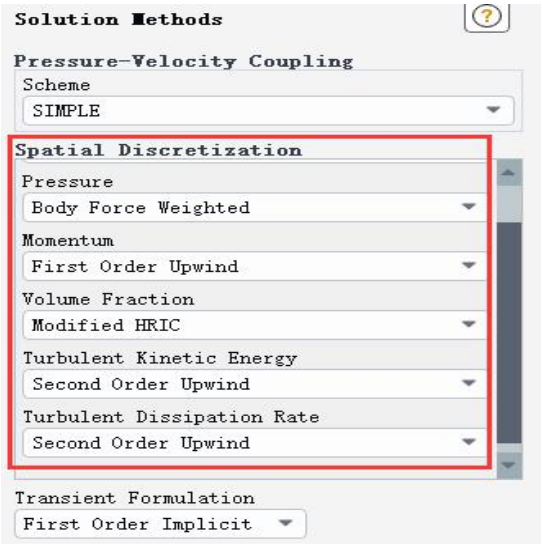

Fig.35: The setting of solution methods

Keeping other settings same as the first case, and then run the simulation calculation, after almost two days of calculation, the calculation is completed. The data measured by the wave probe is processed. For the second test case, the time evolution of a focused wave along the numerical wave tank is shown in Figure 34. It looks well the phenomenon of wave focusing in time along with the numerical wave tank. However, from the Figure 36, remaining plots of free surface elevations at WP5-8 presented in Appendix A3. By comparing with the experimental data, it can be found that the peak of elevation appearance keep the same time with experiment data at different positions. In addition, the shape of the free surface elevation is also very similar with experiment. But unfortunately, the maximum amplitude of the elevation is much smaller than the experimental data. So the second test case also didn't have a good agreement with experiment data, which means that the NWT was not able to reproduce the focused waves tested experimentally, the improvement of NWT is required when we use it to validate the wave flume.

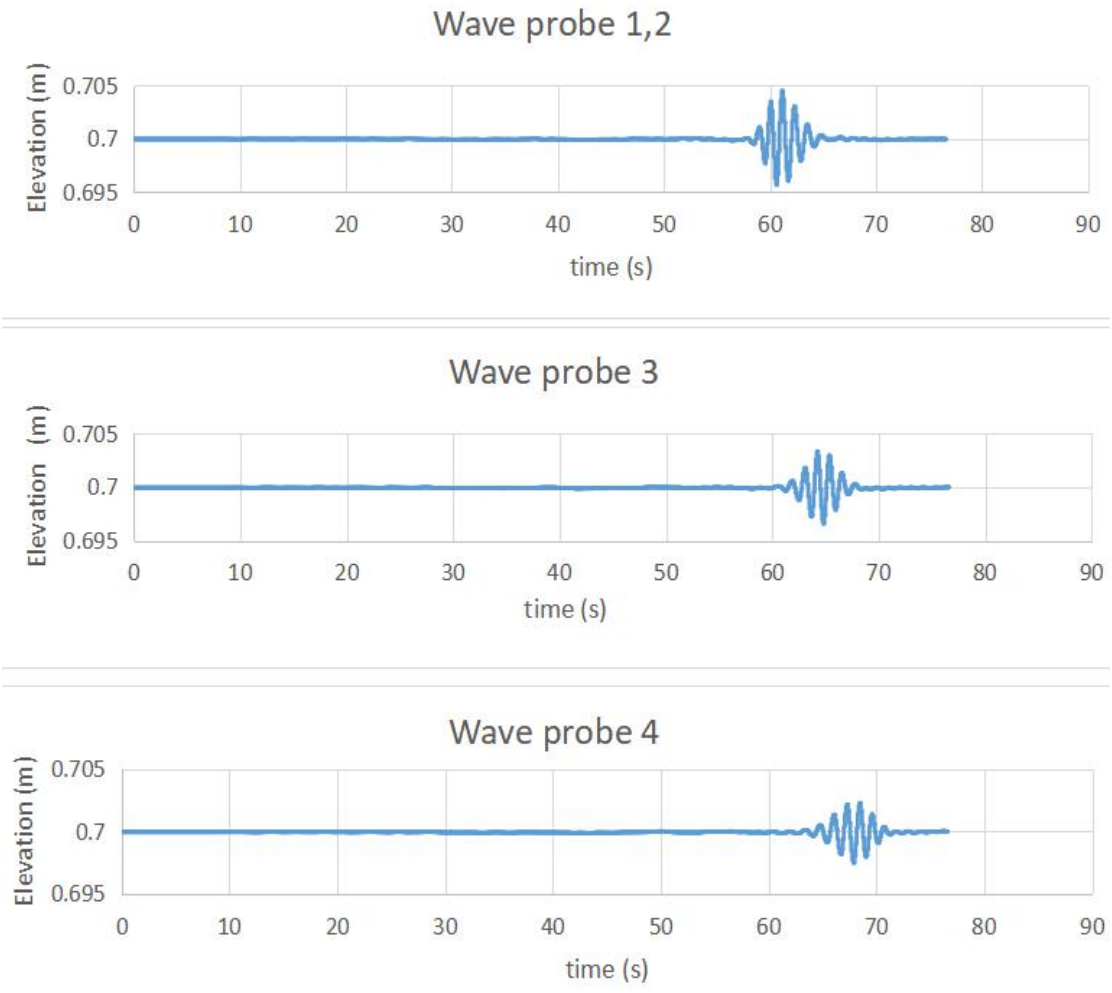

Fig. 36: Time trace of a focused wave at three different locations

For the second test case, the experimental and simulation free surface elevations are compared for WP3 as well. The comparison of experiment data and simulation result are presented in Figure 37.

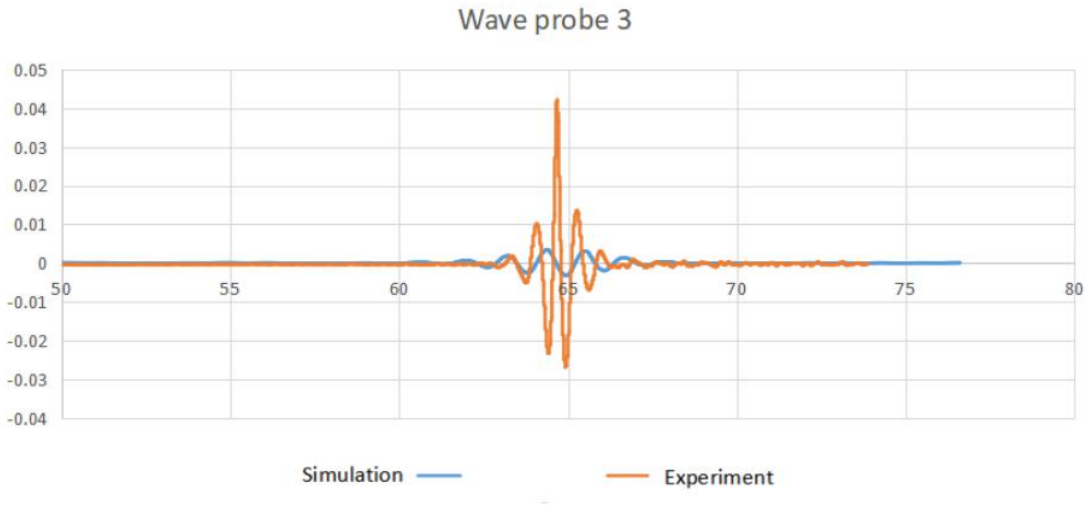

Fig. 37: Comparison of simulation and experiment for WP3 for second case

To get a better understanding of the origins of the difference observed from the Figure 37, the spectrum analysis of the simulation signal was performed for WP3. It can be seen that the energy densities of the frequency components are smaller in the experimental result. This test case is unsuccessful as well. The wave elevation and its spectrum for WP3 is shown in Figure 38.

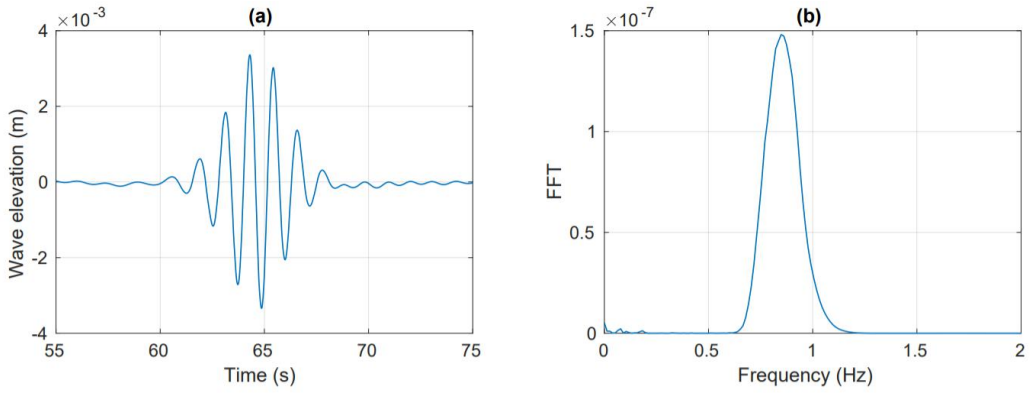

Fig.38: The wave elevation and its spectrum for WP3 in the second case

After comparing the two test cases with the experimental results, it can be found that the focused wave can be generated relatively well, and there is good agreement in time and shape, but the height of elevation for the two test cases have quite big error compared with the experimental results. So the NWT couldn't reproduce accurately the measured and computed wave kinematics. The reasons for this result are analyzed. The first possible reason is that there have problem in the selection of the turbulence

model and the solver, and the second is the mismatch between the time step selection and the volume fraction parameters. The specific reasons need more time to verify, which will be done as future work.

6 Conclusion

This thesis is based on the theory of computational fluid dynamics, using the commercial software Fluent UDF function to build a wave numerical water tank, using dynamic grid technology to simulate the motion of the wave maker, and using the VOF model to simulate the free surface.

First of all, we use the generation of regular waves as test cases. When the wave shape we expect is generated in the numerical wave tank, the stability and reliability of the wave-maker were proved, then we start to simulate the focused wave.

For focused wave, the experimental results from a test campaign conducted in July 2018 in the COAST laboratory in Plymouth University, UK, were used to validate the accuracy of the numerical model. In the numerical simulation, the wave tank is 35 m long with a water depth of 0.7 m. Spatial discretization in the horizontal direction Δx is adopted as 0.014 m, and the time step Δt is 0.005 s. The total simulation duration is 80s.

As we know that the experiment wave flume have some inherent errors for example, reflections, accuracy of the measuring equipment, etc. Therefore, the numerical wave tank is not to accurately reproduce experimental waves, but to generate similar waves in terms of period and shape of free surface elevation. At addition,comparison of the free surface elevations at different locations between the numerical results and experimental data is presented in figure 31 and figure 35. It can be observed that the numerical results did not have a good agreement with the experimental data along the wave tank to reproduce the process of the wave focusing accurately.

References

[1] HANNAH RITCHIE,MAX(2018)
World wide energy consumption
https://ourworldindata.org/grapher/global-primary-energy?stackMode=relative

[2] Titah-Benbouzid, Hosna, and Mohamed Benbouzid. "Ocean wave energy extraction: Up-to-date technologies review and evaluation." 2014 International Power Electronics and Application Conference and Exposition. IEEE, 2014.

[3] Drew, Benjamin, Andrew R. Plummer, and M. Necip Sahinkaya. "A review of wave energy converter technology." (2009): 887-902.

[4] N. Veritas, Environmental conditions and environmental loads, Det Norske Veritas (2000).

[5] Wikipedia website
https://en.wikipedia.org/wiki/Wave_tank\.(online)

[6] Alix Untrau's report: "Kinematics of regular and focused waves:an experimental and numerical study".

[7] C. Windt, J. Davidson, J. Ringwood, High-fidelity numerical modelling of wave energy systems: A review of computational fluid dynamics-based numerical wave tanks, Renewable and Sustainable Energy Reviews (2018).

[8] C. Windt, J. Davidson, P. Schmitt, J. Ringwood, On the assessment of numerical wave makers in cfd simulations, Journal of Marine Science and Engineering (2019).

[9] Sreenivas Jayanti (2018): Computational Fluid Dynamics for Engineers and Scientist Springer.

[10] Josh Davidson, Marie Cathelain, Louise Guillemet, Thibault Le Huec& John V. Ringwood (2015):Implementation of an OpenFOAM Numerical Wave Tank for Wave Energy Experiments Proceedings of the 11th European Wave and Tidal Energy Conference 6-11th Sept.2015, Nantes, France pp.(09B1-1-1)-(09B1-1-10).

[11] Gomes, M. das N., et al. "Computational modeling of a regular wave tank." 2009 3rd Southern Conference on Computational Modeling. IEEE, 2009.

[12] Xu G, Hao H, Ma Q, et al. An Experimental Study of Focusing Wave Generation with Improved Wave Amplitude Spectra[J]. Water, 2019, 11(12): 2521.

[13] ANSYS HELP ONLINE
https://ansyshelp.ansys.com/?ReturnUrl=%2FViews%2FSecured%2Fcorp%2Fv195%2Fflu_ug%2Fflu_ug_sec_pp_trans.html%3Fq%3DVelocity%20profile%20method (online).

[14] Wikipedia website
https://en.wikipedia.org/wiki/Courant%E2%80%93Friedrichs%E2%80%93Lewy_condition.(online).

[15] https://www.simscale.com/blog/2017/08/cfl-condition/(online).

APPENDIX

A.1. Free surface elevations at WP5-8 for focused waves from experiment data

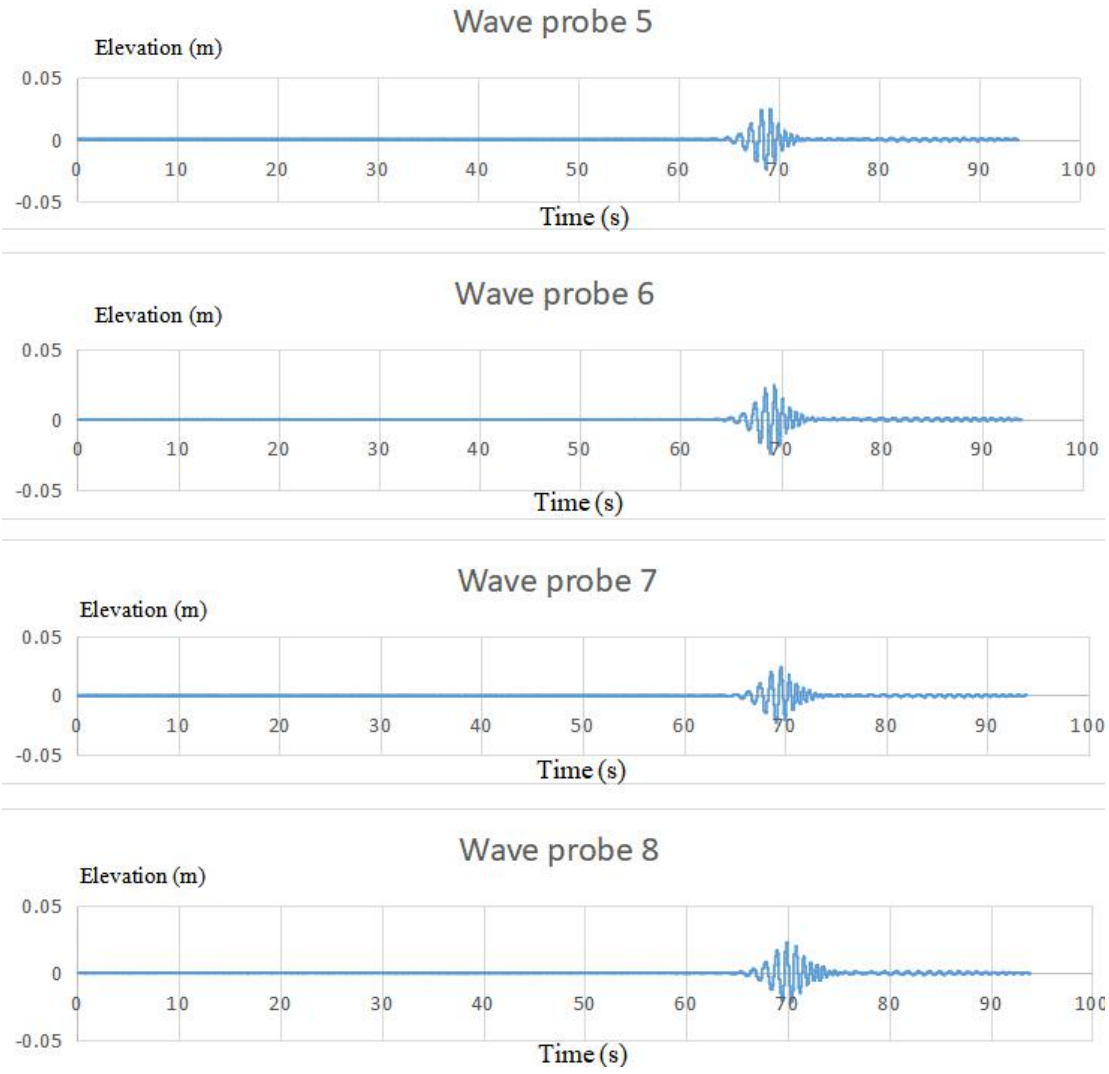

A.2. Free surface elevations at WP5-8 for focused waves from simulation data for first test case.

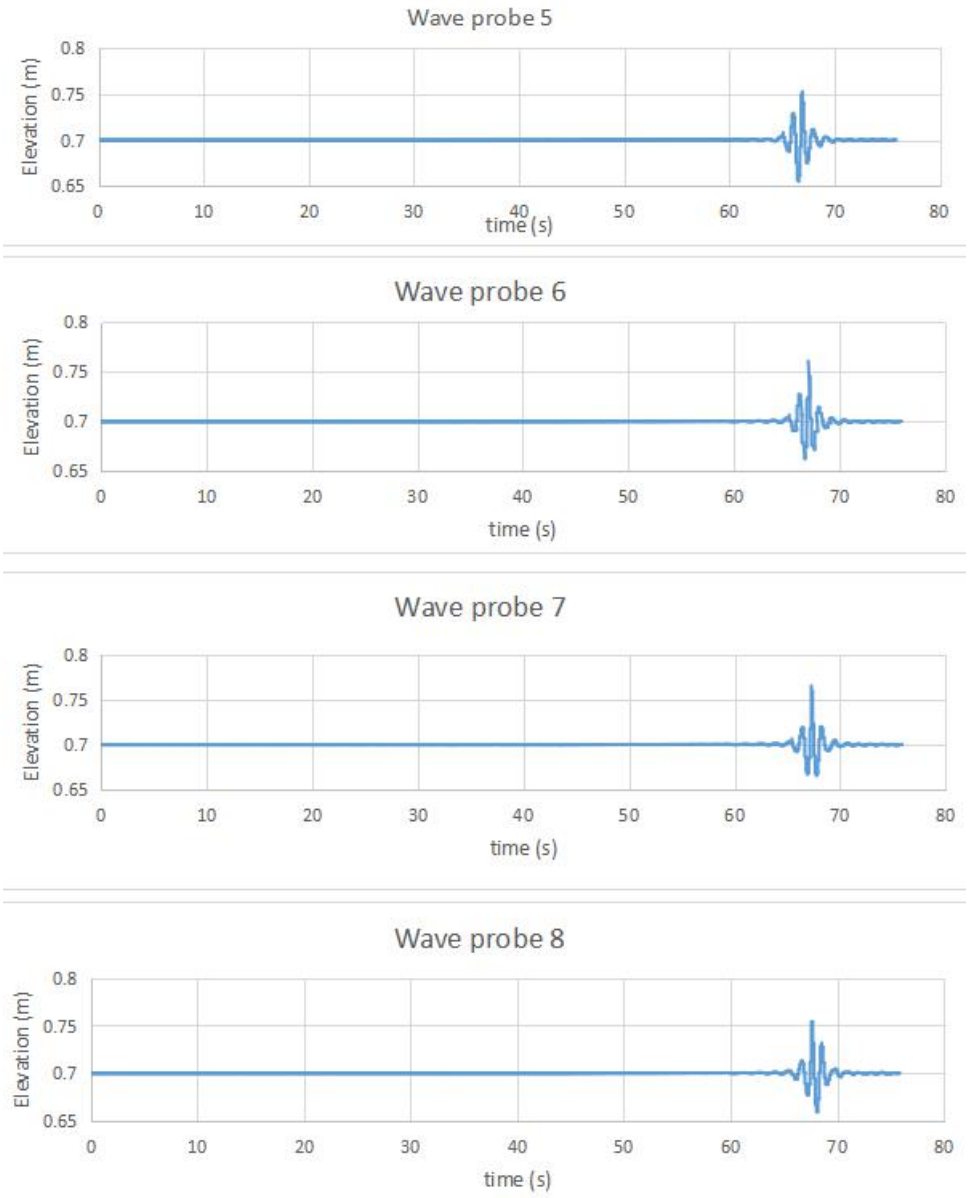

A.3. Free surface elevations at WP5-8 for focused waves from simulation data for second test case.